ACS Biomaterials SCIENCE & ENGINEERING

pubs.acs.org/journal/abseba

Article

Engineered Gold and Silica Nanoparticle-Incorporated Hydrogel Scaffolds for Human Stem Cell-Derived Cardiac Tissue Engineering

Hamid Esmaeili, Alejandra Patino-Guerrero, Ronald A. Nelson, Jr., Nina Karamanova, Taylor M. Fisher, Wuqiang Zhu, François Perreault, Raymond Q. Migrino, and Mehdi Nikkhah*

Cite This: *ACS Biomater. Sci. Eng.* 2024, 10, 2351−2366

Read Online

ACCESS | Metrics & More | Article Recommendations | Supporting Information

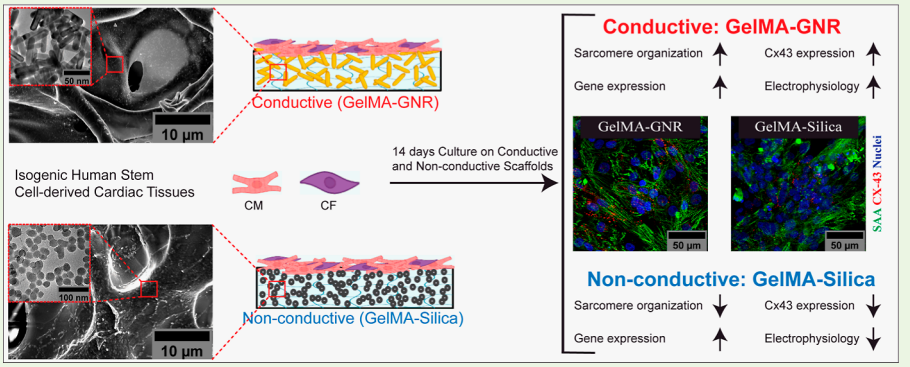

ABSTRACT: Electrically conductive biomaterials and nanomaterials have demonstrated great potential in the development of functional and mature cardiac tissues. In particular, gold nanomaterials have emerged as promising candidates due to their biocompatibility and ease of fabrication for cardiac tissue engineering utilizing rat- or stem cell-derived cardiomyocytes (CMs). However, despite significant advancements, it is still not clear whether the enhancement in cardiac tissue function is primarily due to the electroconductivity features of gold nanoparticles or the structural changes of the scaffold resulting from the addition of these nanoparticles. To address this question, we developed nanoengineered hydrogel scaffolds comprising gelatin methacrylate (GelMA) embedded with either electrically conductive gold nanorods (GNRs) or nonconductive silica nanoparticles (SNPs). This enabled us to simultaneously assess the roles of electrically conductive and nonconductive nanomaterials in the functionality and fate of human-induced pluripotent stem cell-derived cardiomyocytes (hiPSC-CMs). Our studies revealed that both GNR- and SNP-incorporated hydrogel scaffolds exhibited excellent biocompatibility and similar cardiac cell attachment. Although the expression of sarcomere alpha-actinin did not significantly differ among the conditions, a more organized sarcomere structure was observed within the GNR-embedded hydrogels compared to the nonconductive nanoengineered scaffolds. Furthermore, electrical coupling was notably improved in GNR-embedded scaffolds, as evidenced by the synchronous calcium flux and enhanced calcium transient intensity. While we did not observe a significant difference in the gene expression profile of human cardiac tissues formed on the conductive GNR- and nonconductive SNP-incorporated hydrogels, we noticed marginal improvements in the expression of some calcium and structural genes in the nanomaterial-embedded hydrogel groups as compared to the control condition. Given that the cardiac tissues formed atop the nonconductive SNP-based scaffolds (used as the control for conductivity) also displayed similar levels of gene expression as compared to the conductive hydrogels, it suggests that the electrical conductivity of nanomaterials (i.e., GNRs) may not be the sole factor influencing the function and fate of hiPSC-derived cardiac tissues when cells are cultured atop the scaffolds. Overall, our findings provide additional insights into the role of electrically conductive gold nanoparticles in regulating the functionalities of hiPSC-CMs.

KEYWORDS: *cardiac tissue engineering, hiPSC-CM, electrically conductive hydrogels, gold nanorods (GNRs), cardiac maturation*

1. INTRODUCTION

Cardiovascular diseases (CVDs), including myocardial infarction (MI), are the major cause of death globally.[1] The human left ventricle (LV) contains approximately 4 billion cardiomyocytes (CMs), and an incident of MI can kill ∼25% of these cells within a short period of time.[2] The adult human heart possesses a limited regenerative potential, where the CM annual renewal

Received: August 30, 2023
Revised: January 17, 2024
Accepted: January 18, 2024
Published: February 7, 2024

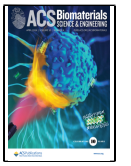

https://doi.org/10.1021/acsbiomaterials.3c01256
ACS Biomater. Sci. Eng. 2024, 10, 2351−2366

rate has been reported to be less than 0.5%,[3] which is insufficient to compensate for the loss of CMs post-MI. Concomitant with this massive CM necrosis is the generation of a fibrotic scar within the myocardium upon MI.[4] This fibrotic tissue results in an increased electrical resistance leading to delayed local electrical signal propagation that could potentially lead to arrhythmia.[5] Therefore, replenishing the lost CMs and restoring the normal electrical activity feature of an infarcted myocardium are crucial steps toward MI repair and regeneration.

Tissue engineering and cell-based cardiac therapies have been offered as promising strategies for the repair of injured myocardium.[6−8] Early efforts for MI repair relied on the delivery of a class of progenitor or stem cells including bone marrow mononuclear cells, skeletal myoblasts (SMs), hematopoietic stem cells (HSCs), endothelial progenitor cells (EPCs), and mesenchymal stem cells (MSCs) through bolus injection of the cells into the target infarcted tissue zone via a catheter or syringe.[9] In recent years, human embryonic stem cells (hESCs) and human-induced pluripotent stem cells (hiPSCs) have been shown to successfully differentiate into bona fide cardiac cells *in vitro*.[10] To date, differentiated CMs from hESCs and hiPSCs have been employed in multiple preclinical studies to generate cardiac muscle-like tissues as emerging candidates for MI repair due to their immense potential for patient-specific therapy and personalized medicine.[11,12] Recent studies have demonstrated that intramyocardially delivered hESC-CMs into the infarcted heart of a nonhuman primate model of MI resulted in the engraftment of cells and extensive remuscularization. Despite these promising findings, ventricular arrhythmias were detected in some of the treated animals.[11] In another study using a nonhuman MI model, injection of allogenic hiPSC-CMs enhanced cardiac contractile function with no evidence of tumor formation and immune rejection.[12] However, compared with the vehicle-treated hearts, ventricular tachycardia was significantly increased in the hearts transplanted with hiPSC-CMs. Overall, these studies and so many others have demonstrated the tremendous promise of stem cell therapy in enhancing cardiac function and regeneration; however, the success of these approaches has been limited due to observed arrhythmias in preclinal studies.[13]

In order to enhance cardiac function and regeneration post-MI, several strategies such as acellular and cell-laden injectable biomaterial scaffolds have been implemented.[14] Examples of the utilized scaffolds include fibrin,[15,16] collagen,[17,18] alginate,[19,20] poly(ethylene glycol) (PEG)-based copolymers,[21] and poly(*N*-isopropylacrylamide) (PNIPAAm).[22] However, the first generation of biomaterial scaffolds often lacked the electrical conductivity features required to enhance the dissemination of electrical signals in the infarcted zone of the myocardium.[23] Since delayed conduction velocity could lead to asynchronous contraction of the heart,[23,24] in recent years there have been tremendous efforts to generate new classes of biomaterial scaffolds offering electrical conductivity features resembling healthy cardiac tissues.[25]

Electrically conductive biomaterial scaffolds have often been designed through the incorporation of conductive components such as carbon-based (i.e., reduced carbon nanotubes)[26−30] and gold nanomaterials (i.e., gold nanorods and gold nanowires)[25] or alternatively electrically conductive polymers (i.e., polyaniline).[24,31] Among these candidates, gold nanoparticles such as gold nanowires (GNWs) and gold nanorods (GNRs) have attracted notable attention due to their ease of fabrication, biocompatibility, ease of surface functionalization, and stable electrical conductivity.[32,33] In a pioneering study, Dvir et al.[34] designed an electrically conductive cardiac tissue by physically mixing GNWs (∼1 μm long) with nonconductive alginate hydrogel. The cultured neonatal rat left ventricular myocytes (NRVMs) on the electrically conductive scaffolds exhibited improved the expression of connexin-43 (Cx43), sarcomeric alpha-actinin (SAA), and cardiac troponin I (cTnI). In recent studies, GNRs incorporated into gelatin methacrylate (GelMA)[35−38] and collagen[39] have also been shown to promote the maturation of NRVMs, as indicated by enhanced expression of SAA and Cx43. Despite their significance, most previous studies have mainly utilized nonhuman cells (i.e., primarily NRVMs) for engineering cardiac tissues. However, hPSC-CMs offer a promising cell source for developing humanized cardiac tissues, enabling more in-depth mechanistic studies and improved clinical translational relevance. Therefore, there is a need for more comprehensive investigations to better understand the role of electrically conductive gold nanoparticles in enhancing the functionality of stem cell-derived CMs, particularly hiPSC-CMs.

In this study, we developed and characterized two classes of nanoengineered hydrogel scaffolds, namely, electrically conductive ones incorporating GNRs and nonconductive ones incorporating SNPs within GelMA hydrogels for cardiac tissue engineering applications. Our specific objective was to assess the impact of these nanomaterial-embedded hydrogels, whether conductive or nonconductive, on the function and fate of hiPSC-CMs when cells are seeded on top of the hydrogel matrices. To achieve this, we employed a comprehensive array of tissue-level, cellular-level, and molecular-level assays, including immunofluorescence (IF) staining, Western blot analysis for protein expression, gene expression profiling, and electrophysiological assessments, such as calcium transients and contractility measurements. Overall, our study and its findings provide valuable insights, suggesting that the electrical conductivity of nanomaterial-embedded hydrogels may not be the sole factor governing the functionalities of hiPSC-CMs when cells are seeded on top of these nanoengineered hydrogels.

2. MATERIALS AND METHODS

2.1. Materials. The list of the used materials is summarized in Table S1.

2.2. Methods. *2.2.1. Gold Nanorod Synthesis and Characterization.* The seed-mediated growth method was used to synthesize GNRs as described previously,[40] with a slight modification as depicted in Figure S1. To prepare the seed solution, 2 mL of CTAB solution (0.2 M, 30 °C) was mixed with 2 mL of $HAuCl_4$ (0.5 mM, 30 °C) under constant stirring. To the stirred solution, ice-cold $NaBH_4$ (240 μL, 0.01 M) was added at once and vigorously stirred at room temperature for 2 min, which resulted in a brownish-yellow solution. To ensure complete degradation of $NaBH_4$, the seed solution was further maintained for 2 h at 30 °C without agitation. To prepare the growth solution, $AgNO_3$ (1.1 mL, 0.0045 M, 30 °C) was added to the CTAB solution (20 mL, 0.2 M, 30 °C) and gently mixed. $HAuCl_4$ (20 mL, 1 mM, 30 °C) was added to this solution followed by gentle mixing, which immediately resulted in a deep yellow solution. Then, 280 μL ascorbic acid (0.0788 M, 30 °C) was added and gently mixed which immediately resulted in a colorless solution. Lastly, the seed solution (48 μL, 30 °C) was added to the growth solution and kept at 30 °C for 24 h. After 30−60 min, the solution color changed to maroon. Upon formation, the GNRs were collected in the Eppendorf tubes and centrifuged at 12,000*g* for 10 min. Further removal of CTAB was achieved by resuspending the GNRs in DI water followed by centrifugation for 10,000*g* for 15 min. Filter DI water (0.1 μm) was used throughout the GNR synthesis.

https://doi.org/10.1021/acsbiomaterials.3c01256
ACS Biomater. Sci. Eng. 2024, 10, 2351−2366

UV−vis−NIR extinction spectra were recorded by using a spectrophotometer (BioTek Synergy H1 Plate Reader) to analyze the surface plasmon resonance (SPR) of the synthesized GNRs. Transmission electron microscopy (TEM) characterization of the GNRs was recorded on a TEM/STEM (2010F-JEOL) with an operating voltage of 200 kV. The diameter and length of at least 800 GNRs from five TEM images were calculated via ImageJ software. A batch of synthesized GNRs was serially diluted, and the optical density for each of the dilutions was analyzed at 400 nm. Inductively coupled plasma mass spectrometry (ICP-MS) was conducted on the samples to quantify the gold content in the unknown samples with a known optical density. Then, the gold content in each sample was plotted against its optical density to generate a standard curve for the GNR concentration measurement.

2.2.2. Gelatin Methacrylate Synthesis and Characterization. GelMA was synthesized according to a previously established protocol.[41] Briefly, gelatin was dissolved in PBS with a concentration of 10% (w/v) at 50 °C under vigorous stirring for ∼1 h until fully dissolved. While stirring vigorously, methacrylate anhydride (MA) (0.8 mL/gram of used gelatin) was slowly added and vigorous stirring was continued at 50 °C for another 3 h. After the completion of the reaction, the solution was aliquoted into 50 mL conical tubes followed by centrifugation at room temperature for 3 min at 3500*g* to remove the unreacted MA. The clear solution was decanted and collected into a glass beaker and kept at 40 °C. Then, two volumes of prewarmed PBS (40 °C) were used to dilute the solution. While the solution was kept under stirring, it was transferred into a dialysis membrane (12 kDa MWCO) and dialyzed against DI water. The DI water was changed twice a day for 7 days. Then, the pH of the solution was adjusted by using 1 M $NaHCO_3$. The solution was filtered (0.2 μm) and divided into 50 mL conical tubes and maintained at −80 °C overnight. Finally, the frozen GelMA solution was lyophilized for 1 week and stored at −20 °C.

2.2.3. Synthesis of GelMA-GNR and GelMA-SNP Hydrogel Scaffolds. Three groups of hydrogels, namely, GelMA-pristine (**GelMA**), GelMA-GNR (GelMA hydrogel embedded with 1.0 mg/mL of GNRs) (**G-GNR**), and GelMA-SNP (GelMA hydrogel embedded with 1.4 mg/mL of SNPs) (**G-SNP**) were fabricated to conduct our experiments as follows. Due to the molecular weight differences between SNPs and GNRs, 1.4 mg/mL of SNPs was considered as the nonconductive control group which contains an approximately similar number of particles in comparison to 1.0 mg/mL of GNRs. The SNPs (5 mg/mL) were dispersed in PBS with a sonication probe. The GNRs were first centrifuged at 10,000*g* for 15 min, and the pellets were dispersed in 7% GelMA hydrogels via 1 h of sonication in a water bath. Then, the Irgacure 2959 (photoinitiator) (1.0% w/v) was dissolved in PBS (50 °C) followed by filtration (0.2 μm) to eliminate the impurities. Certain amounts of GNRs (1.0 mg/mL) and SNPs (1.4 mg/mL) were mixed with the GelMA prepolymer solutions and balanced with PBS so that the final concentration of Irgacure 2959 and GelMA in each group was 0.5 and 15% w/v, respectively. The prepared prepolymer solutions were sonicated in a water bath for 1 h to further enhance the dispersion of nanoparticles. Then, these prepolymer solutions were used to fabricate thin (150 μm) hydrogel scaffolds. The UV source (360−480 nm) was placed at 8 cm from the hydrogel films, resulting in an intensity of ∼7.64 mW/cm^2. The prepolymer solution (30 μL) was added between two 150 μm spacers and a TMSPMA-coated round glass slide was placed on top. The hydrogel films were formed by UV cross-linking for 20, 50, and 35 s for GelMA, G-GNR, and G-SNP, respectively.

2.2.4. Characterization of GelMA-based Hydrogel Scaffolds. The mechanical property of the synthesized GelMA-based hydrogel scaffolds was analyzed through the measurement of compressive modulus. 100 μL of prepolymer solutions were placed between two 500 μm spacers, covered by a glass slide, and exposed to 7.64 mW/cm^2 UV light (360−480 nm) for various time points. Then, samples were separated from the slide and incubated in PBS overnight at 37 °C. The 8 mm punched gels were blotted and measured at a rate of 13 μm/s on an Instron machine (Instron 5943, 50 N load cell). The compressive modulus of the samples was evaluated by the slope of the linear region corresponding to 0−5% strain.

For electrical conductivity characteristics, 150 μm thick hydrogel scaffolds were prepared as above, and a two-probe measurement method with an electrochemical impedance spectroscopy (EIS) potentiostat was used to evaluate their impedance. Specifically, at a 10 mV applied voltage, the impedance of each biomaterial was analyzed from 1.0 Hz to 100 kHz.

Scanning electron microscopy (SEM) imaging (Zeiss Auriga) was utilized to evaluate the ultrastructure and porosity of the lyophilized hydrogel scaffolds. The hydrogel scaffolds were frozen in liquid nitrogen, lyophilized, coated with carbon, and imaged at 5 kV. Energy-dispersive X-ray spectroscopy (EDS) was also employed to evaluate the elemental component in the hydrogel scaffolds.

2.2.5. Human iPSC-Cardiomyocyte Differentiation. Human induced pluripotent stem cells (hiPSCs) (IMR90-4, WiCell) were cultured on Matrigel-coated six-well plates in the mTeSR1 medium. The cells were passaged upon reaching ∼80% confluency. The used medium was aspirated, and the cells were gently washed with PBS followed by dissociation with 0.5 mM EDTA (1 mL per well) for ∼6 min. Then, after EDTA removal, 1 mL of mTeSR1 medium was used to mechanically detach the cells and plate on a separate Matrigel-coated well.

The GiWi differentiation protocol, with slight modification, was used to differentiate hiPSCs into hiPSC-CMs (hiCMs).[10,42−44] Specifically, hiPSCs were plated on Matrigel-coated six-well plates with a specific seeding density (∼0.1 M per well). Upon ∼85% cell confluency, the mTeSR1 medium was replaced with RPMI/B27 without insulin medium (4 mL) supplemented with 8 μM GSK3-β inhibitor CHIR99021 (CHIR) and maintained for 24 h. After 24 h, the CHIR-containing culture medium was changed with RPMI/B27 without insulin (5 mL) for 48 h (until day 3). On day 3, the medium was changed to a 1:1 ratio of RPMI/B27 without insulin (2.5 mL) and the conditioned medium (2.5 mL) supplemented with 5 μM Wnt inhibitor IWP2 and maintained for another 48 h. On day 5, the medium was changed to RPMI/B27 without insulin (5 mL) and left for another 48 h (until day 7). On day 7, the old medium was removed, and RPMI/B27 (with insulin) (5 mL) was added and replenished every other day. The spontaneous beating of hiCMs was normally observed on day 11 of differentiation. Purification of the hiCMs was achieved through a glucose-depleted culture medium containing lactate.[45] At day 13 postdifferentiation, the medium was switched to the glucose-depleted RPMI/B27 (with insulin and 5 mM sodium L-lactate) medium (5 mL), and the medium was changed every 3 days until day 19. On day 19, the medium was changed to RPMI/B27 (with insulin) medium (5 mL) again. Before using the differentiated hiCMs to form the cardiac tissues, hiCMs were maintained in a 2 mL of serum- and supplement-free medium for another 24 h to synchronize their cell cycle. 25 to 28 days old hiCMs were used throughout the experiments.

2.2.6. Human iPSC-Cardiac Fibroblast Differentiation. hiPSC-derived cardiac fibroblasts (hiPSC-CFs) (hiCFs) were generated using an established protocol with a slight modification.[46] Briefly, hiPSCs (IMR90-4) were dissociated with 1 mL/well EDTA (0.5 mM in PBS) solution at room temperature for ∼6 min and plated on Matrigel-coated wells at the density of 0.1−0.15 × 10^6 cells per well of six-well plates in mTeSR1. Cells were maintained in mTeSR1 for 3 to 4 days, and the medium was changed daily until reaching 80−90% confluence. On day 0, the medium was changed to 4 mL of insulin-free RPMI/B27 containing 7 μM CHIR99021. After 24 h (day 1), the medium was replaced by 5 mL of insulin-free RPMI/B27 and maintained for another 24 h (day 2). Then, the media were removed and 2.5 mL of hiCF differentiation medium (hCFBM) containing 70 ng/uL bFGF was added per well for another 48 h (day 4). After day 4, cells were supplied with 2.5 mL hCFBM supplemented with 70 ng/uL bFGF every other day until day 20 when cells were passaged and cryopreserved for later uses. After day 20, the differentiated hiCFs were either cryopreserved or passaged and maintained in FGM3 media.

2.2.7. Formation of Cardiac Tissues. To form the cardiac tissues, a 100 μL suspension of isogenic hiCMs and hiCFs (7:1) containing 0.4 M cells was dropped on a thin layer (150 μm) of hydrogel scaffolds and

https://doi.org/10.1021/acsbiomaterials.3c01256
ACS Biomater. Sci. Eng. 2024, 10, 2351−2366

incubated at 37 °C for ∼2.5 h. Then, the rest of the medium was gently added to the wells ensuring the coverage of the hydrogel scaffolds and maintained for 2 weeks in culture. The medium was replenished every other day.

2.2.8. Cell Viability Assay. A Live/Dead kit (Life Technology, USA) was used according to the kit instructions. hiCMs and hiCFs. 0.4 M hiCF and hiCM (7:1) hiCFs were seeded on hydrogel scaffolds for 3 days and gently washed once with 1× PBS. The tissues were kept in a solution of 4 μM EthD-1 and 2 μM calcein-AM for 20 min at room temperature. Then, the samples were washed with 1X PBS before imaging.

2.2.9. Immunofluorescence Staining. On day 14 of the culture, cardiac tissues were washed once with 1× PBS followed by fixing in paraformaldehyde (4%) for 15 min at room temperature. Then, the samples were washed three times with PBS-glycine for 10 min of incubation at room temperature. The cells were then permeabilized with Triton-X-100 (1%) for half an hour at room temperature. Next, the tissues were blocked with a solution of goat serum in PBS-tween-20 (10%) at room temperature for 1 h. Next, the primary antibodies were diluted in the same blocking solution and added to the cardiac tissues followed by overnight incubation at 4 °C. The primary antibodies used in this study were as follows: rabbit monoclonal anti-vimentin (1:100), mouse monoclonal anti-Troponin T (TnT) (1:100), Alexa Fluor 488 Phalloidin (1:40), mouse monoclonal anti-integrin β1 (1:250), mouse monoclonal anti-sarcomeric alpha-actinin (1:100), and rabbit polyclonal anti-connexin 43 (1:100). After overnight incubation, the tissues were washed at room temperature five times with PBS-tween-20 (10 min of incubation). The secondary antibodies were diluted in the 4′,6-diamidino-1-phenylindole (DAPI) (1:1000) followed by centrifugation at 18,800*g* for 10 min to pellet the aggregates and impurities. The tissues were then stained with secondary antibodies for 1 h at room temperature. In this study, Alexa Fluor 647 goat anti-rabbits (1:500), Alexa Fluor 488 goat anti-rabbits (1:500), Alexa Fluor 647 goat anti-mouse (1:500), and Alexa Fluor 488 goat anti-mouse (1:500) were used as secondary antibodies. 40× and 63× magnification imaging were performed with confocal imaging for the samples stained with SAA/Cx43 and F-actin/Integrin, respectively. Other stained samples were analyzed via a Zeiss microscope (Observer Z1) equipped with Apotome2 at 10× and 20× objectives. Finally, ImageJ software was used to process the *z*-stack images.

Similar to a recent publication,[47] to assess the sarcomere quality (coverage and striation) of the cardiac tissues formed on the hydrogel scaffolds, we defined a metric where IF images stained with sarcomeric alpha-actinin were divided into nine sections and the sarcomere quality of each square was scored from 0 for the lowest quality to 10 for the highest quality region. Then, the total value for each image was divided by 9 to get the average qualitative score for each image. The average values for each biological replicate were then averaged to get the aggregated qualitative score for all of the biological replicates.

2.2.10. Western Blot for Protein Expression. Fourteen days old cardiac tissues were washed once with 1× PBS and complete RIPA buffer containing protease and phosphatase inhibitors, and dithiothreitol (DTT) (Millipore SIGMA) was used to prepare cell lysates. Proteins from the whole lysates were quantified with Bradford Reagent (SIGMA). Analysis of protein content was performed on a PECTRA MAX 190 spectrophotometer (Molecular Devices). Samples (30−40 μg/well) were separated by electrophoresis in precast 4−20% Novex Wedge Well Tris-Glycine Gel (Invitrogen).

The Immune-Blot LF PVDF membrane with a 0.45 μm pore size (BIO-RAD) was used for the protein blotting. The blot was washed in 2× PBS with 0.1% Tween-20 (PBS-T) (SIGMA) followed by incubation for 1.5 h in blocking buffer (4% BSA in 1× PBS-T, pH 7.4) at room temperature with gentle shaking and then probed with primary antibodies overnight at 4 °C with gentle shaking. Rabbit polyclonal anti-connexin 43 (1:5000) and β-Actin (13E5) rabbit IgG (1:1000, Cell Signaling) were used as the antibodies. β-Actin was used as a "housekeeping" protein marker. The next day after the primary antibody application, the blot was washed with 3× TBS-T and probed with the secondary antibody (LI-COR IRDye). LI-COR Odyssey CLX Imaging System was used to visualize proteins and then stripped with NewBlot PVDF Stripping Buffer (LI-COR), washed, and reprobed. Analysis was performed in LI-COR Image Studio, version 4 0, and then exported to Microsoft Excel.

2.2.11. Analyses of Beating Behavior of Cardiac Tissues. Beating behavior of the cardiac tissues were analyzed as described in our recent publications.[48−50] Briefly, cardiac tissue samples were placed on the stage of a Zeiss microscope, and phase contrast images of the cardiac tissues were obtained at days 3, 7, and 14 of culture using a 10× objective. Time-lapse images were acquired (10×) for 20 s on day 14 to examine spontaneous or stimulated contraction of the cardiac tissues. The beating behavior information including beating patterns, beats per minute (BPM), and interbeat interval variability (IIV) were all extracted using a custom-written MATLAB code. To evaluate IIV, the contraction peaks and the correlated times to each peak were extracted from the recorded videos by using the MATLAB code. Then, the standard deviation of the contraction peak times was computed and reported as IIV as a measure of beating regularity.

2.2.12. Gene Expression Analysis. Reverse-transcription quantitative polymerase chain reaction (RT-qPCR) was used to quantify the relative expression levels of a group of cardiac-specific genes. After 2 weeks of culture, the cardiac tissues formed on the hydrogel scaffolds were incubated with prewarmed TrypLE (37 °C) for 10−15 min at 37 °C. RPMI/B27 (with insulin) medium was added to neutralize the TrypLE, and the cells were collected in Eppendorf tubes and centrifuged for 3 min at 300*g*. After removing the supernatant, the pellets were lysed with lysis buffer (350 μL). RNA extraction from the cell lysates was then performed using Quick-RNA MicroPrep Kit (Zymo Research; Cat #R1050) based on the manufacturer's protocol. The RNA purity and concentration were then analyzed by 260/280 nm absorbance using Nanodrop one instrument (Thermo Scientific). Next, iScript Reverse Transcriptase Supermix (BioRad) was used to synthesize cDNA from the extracted RNA. Then, qPCR using the iTaq Universal SYBR Green Supermix (Bio-Rad) was used to analyze the synthesized cDNA. Melt curve analysis and qPCR product size verification were used to validate the designated set of primers, as shown in Table S2. The qTower 2.0 was then used to analyze the qPCR, and the delta−delta Ct method ($2^{-\Delta\Delta Ct}$) with 18S as the housekeeping gene was utilized to quantify the relative gene expression fold change. A suspension of hiCMs and hiCFs at day 0 (D0) before culture on hydrogel scaffolds was used to normalize the relative gene expression levels. The row *Z*-score for each gene was calculated from the fold changes of each experimental group and plotted in an expression heatmap with GraphPad Prism software.

2.2.13. Electrophysiological Analysis of the Cardiac Tissues. External electrical stimulation of the cardiac tissues was performed via a custom-made chamber as described previously.[51] First, two carbon electrodes (3.5 × 0.3 cm) were mounted into a 6 cm Petri dish in a parallel fashion with 1 cm apart. The wires were then attached to the opposite sides of the carbon electrodes, and the connections were sealed with silicon paste. Then, the cardiac tissues were placed between the carbon electrodes and rinsed with RPMI/B27 with insulin. The chamber was then mounted on the microscope stage, and live videos were recorded with external electrical stimulation. Electrical pulse stimulation was performed at 1.0, 1.5, and 2.0 Hz with 2 ms durations using a pulse generator (BK PRECISION 4052).

For calcium transient imaging, 14-day-old tissues were incubated with calcium indicator (Fluo-4-AM in Pluronic) at 37 °C for 45 min and rinsed in Tyrode's solution at 37 °C (25 min). Calcium transient was performed under electrical stimulation with the same setup described for external electrical stimulation. Videos were obtained using a 60 ms exposure time at 16.3 frames per second (fps) using a Zeiss fluorescence microscope at a 488 nm wavelength. To generate calcium spike traces, videos were analyzed using the Fiji software[52] and the background fluorescence intensity was subtracted from the fluorescence intensity of calcium spikes (F) resulting in background-corrected changes in fluorescence values for each frame (ΔF). The ΔF values were divided by the minimum fluorescence intensity of calcium spikes of the same spot to acquire $\Delta F/F_0$ values and plotted against time.[53]

2.2.14. Statistical Analysis. Unless otherwise stated, all quantitative data were presented as means ± standard deviations (S.D.) with three

https://doi.org/10.1021/acsbiomaterials.3c01256
ACS Biomater. Sci. Eng. 2024, 10, 2351−2366

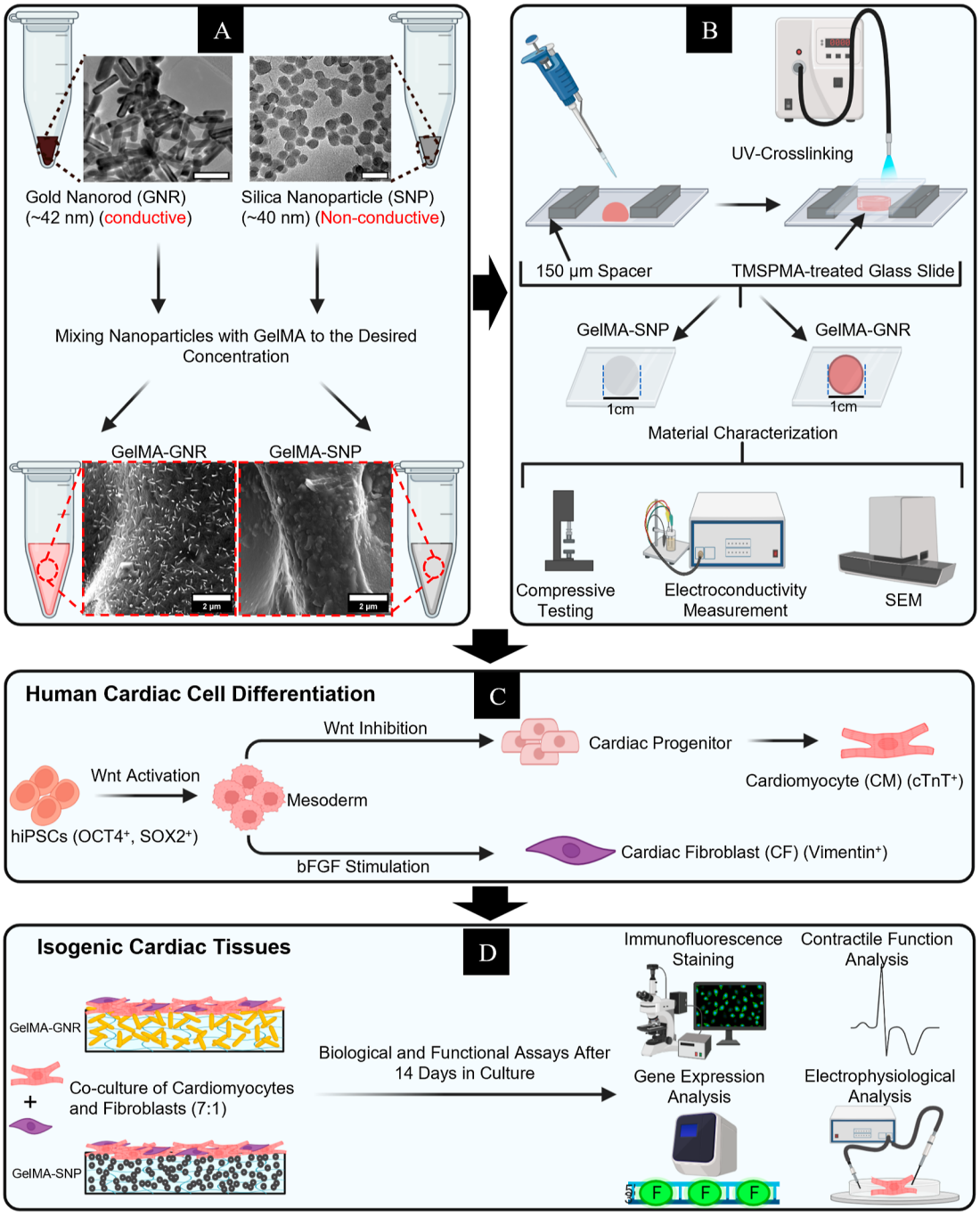

Figure 1. Schematic illustration of fabrication of nanoengineered hydrogel scaffolds and the overall experimental procedure for downstream mechanistic biological studies. (A) Preparation of the prepolymer solutions of G-GNR and G-SNP. TEM images show the dispersed silica nanoparticles (SNPs) and GNRs in PBS. The scale bar in the TEM pictures is 50 nm. The SEM images show the presence and distribution of nanoparticles within the hydrogel scaffolds. (B) Fabrication and characterization of thin (150 μm) hydrogel scaffolds (1 cm diameter) formed with GelMA, G-GNR, and G-SNP prepolymer solutions. Compressive modulus testing, impedance measurement, and SEM imaging were performed to characterize the hydrogel scaffolds. (C) Schematic illustration of hiCFs and hiCMs differentiation from hiPSCs. (D) Formation of isogenic cardiac tissues by culturing a 7:1 ratio of hiCMs to hiCFs on GelMA, G-GNR, and G-SNP hydrogel scaffolds. The cardiac tissues were grown for 14 days, followed by downstream biological and electrophysiological assays.

biological replicates. One-way ANOVA with Tukey's posthoc was performed when the data sets had more than two experimental groups. Student's *t*-test was used for the analysis of data sets with two experimental groups. GraphPad Prism software version 6 was used to evaluate the statistical analyses with *P*-values < 0.05 considered significant.

3. RESULTS AND DISCUSSION

3.1. Fabrication and Characterization of the Nanoengineered Hydrogel Scaffolds. The UV−vis spectra analysis of the synthesized gold nanorods (GNRs) demonstrated the presence of transverse SPR (TSPR) and longitudinal SPR (LSPR) at approximately 520 and 780 nm, respectively (Figure S2A). These resonances correspond to the short and

https://doi.org/10.1021/acsbiomaterials.3c01256
ACS Biomater. Sci. Eng. 2024, 10, 2351−2366

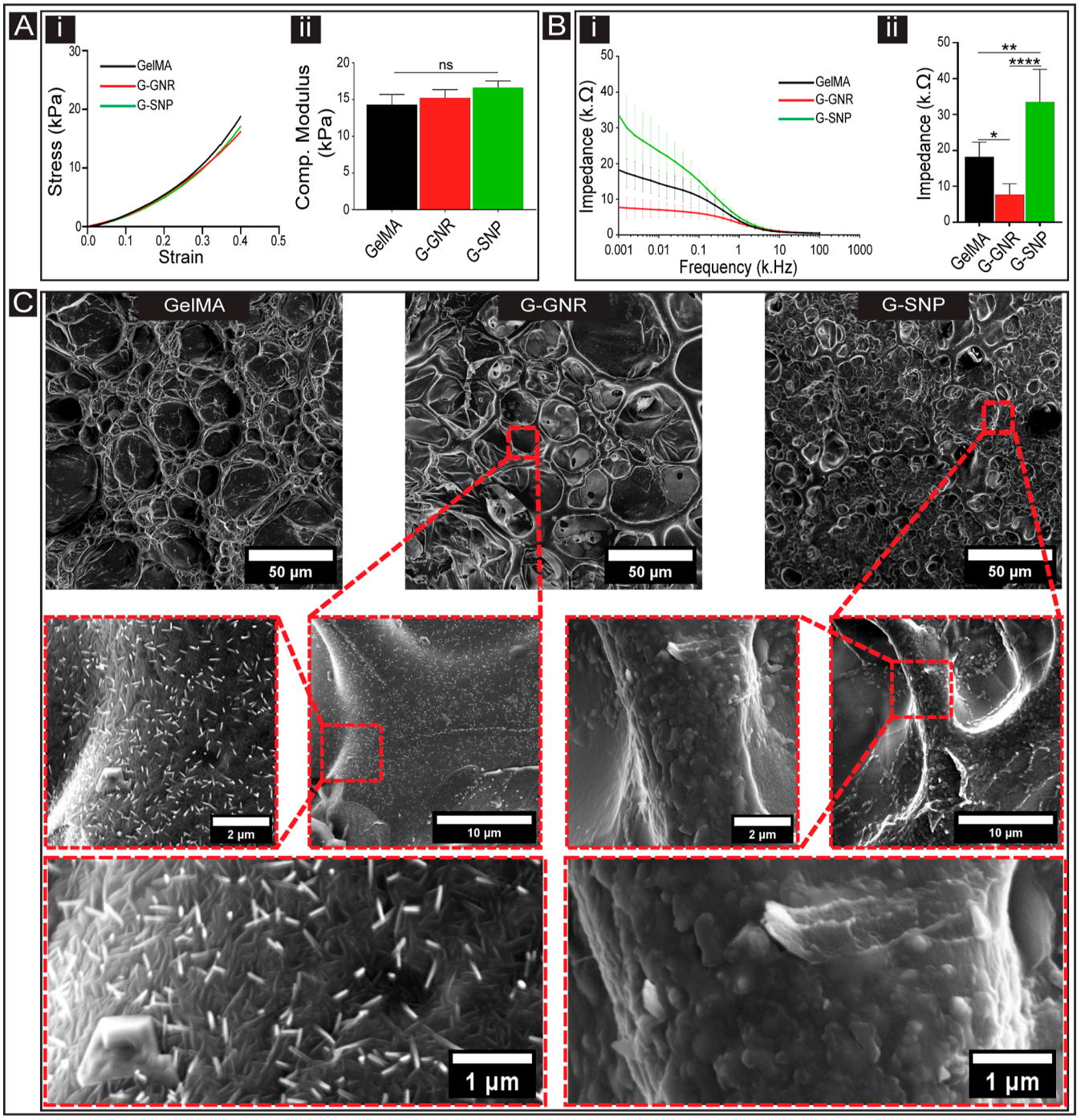

Figure 2. Material characterization of the synthesized nanoengineered hydrogel scaffolds. (A) Representative compressive modulus curves of pure (i.e., pristine) GelMA, G-GNR, and G-SNP measured by an Instron machine (i) and compressive modulus of the hydrogel scaffolds (one-way ANOVA with a Tukey's posthoc test, $n = 4$) (ii). (B) Bode diagram of the hydrogels at various frequencies (i) and impedance of GelMA, G-GNR, and G-SNP hydrogel scaffolds at 1.0 Hz measured by EIS Potentiostat (one-way ANOVA with a Tukey's posthoc test, $n = 6$) (ii). (C) SEM images of GelMA, G-GNR, and G-SNP hydrogel scaffolds. Data were expressed as mean ± standard deviation. *$p < 0.05$, **$p < 0.01$, ****$p < 0.0001$, and ns (not significant).

long axes of the GNRs. The TEM images confirmed the successful formation of GNRs with the desired geometries (Figure S2B). The synthesized GNRs had an average length and diameter of 42.8 ± 4.8 and 11 ± 1.7 nm, respectively, resulting in an aspect ratio of 3.9 ± 0.6 determined by dividing the length by the diameter (Figure S2D,E). For this study, GNRs with an aspect ratio of approximately 4.0 were specifically chosen, consistent with previously published works.[35,38,39] The standard curve generated from ICP-MS data demonstrates a linear relationship between the optical density and the gold content in the GNR solution, as depicted in Figure S2F. Since this curve was established based on the gold content in the GNR solution at 400 nm, the equation derived from it can be used to quantify the gold content of any GNR solution with an unknown concentration by inserting the optical density of the solution into the equation. Furthermore, the homogeneous dispersion of

https://doi.org/10.1021/acsbiomaterials.3c01256
ACS Biomater. Sci. Eng. 2024, 10, 2351−2366

the ∼40 nm silica nanoparticles (SNPs) in DI water was confirmed through TEM images, as shown in Figure S2C. The SNPs were specifically selected as the nonconductive counterpart due to their biocompatibility, similarity in diameter and size to GNRs, and ease of dispersion within the hydrogel scaffolds,[37] providing a suitable nonconductive nanomaterial to conduct our studies. UV−vis spectra analysis performed on the prepolymer solutions confirmed that the sonication step used to enhance the homogeneous GNR dispersion in the hydrogel scaffolds did not result in the fragmentation of GNRs into smaller particles. This was indicated by the TSPR and LSPR of the G-GNR prepolymer solution being consistent with those of the intact synthesized GNRs (Figure S2A). Figure 1 illustrates the schematic depicting the formation of 150 μm thick hydrogel scaffolds (Figure 1A,B), the differentiation protocol for generating isogenic cardiac cells from hiPSCs (Figure 1C), and the subsequent biological studies conducted after the formation of the nanoengineered tissues (Figure 1D).

Compressive testing was conducted to analyze the bulk mechanical properties of the synthesized nanoengineered hydrogel scaffolds. Previous studies have demonstrated that hiPSC-CMs (hiCMs) exhibit enhanced beating and contractility on scaffolds with stiffnesses closer to the physiological range of ∼10−20 kPa.[54] To achieve this desired stiffness range for all hydrogel scaffolds, a series of optimization experiments was conducted. These experiments determined the appropriate UV exposure times for GelMA, G-GNR, and G-SNP hydrogel scaffolds to be 20, 50, and 35 s, respectively (Figure 2A), to match this physiological stiffness. As illustrated in Figure 2A(i), the stress−strain curves for all hydrogel groups overlapped when photopolymerization was performed based on the above-mentioned exposure times, indicating that the hydrogels exhibited similar compressive modulus values. Statistical analyses presented in Figure 2A(ii) further confirm that there were no significant differences in the bulk stiffness values among the hydrogel groups. While the bulk stiffness of the hydrogel substrates was maintained within the same range based on our experimental design, the presence of nanoparticles could have led to localized changes in substrate stiffness, which cardiac cells can sense, as also demonstrated by the previous studies.[39,55] However, in this study, our focus was to assess and dissect the impact of the electroconductivity of GNRs on cardiac cell function while maintaining the hydrogel bulk stiffness the same across the experimental groups.

The Bode diagram illustrates that the impedance magnitude of G-GNR was consistently lower than those of GelMA and G-SNP across the frequency range (Figure 2B(i)). Furthermore, it was observed that at 1.0 Hz, the impedance of G-GNR hydrogel scaffolds was significantly lower compared to the other hydrogels, indicating enhanced conductivity resulting from the incorporation of GNRs (Figure 2B(ii)). Overall, across all samples, the G-GNR scaffolds exhibited the highest electrical conductivity, evident by the lowest impedance values, while the addition of SNPs led to a more insulating hydrogel. In consideration of the experimental design and the selection of scaffold compositions, our three hydrogel candidates (GelMA, G-GNR, and G-SNP), demonstrated well-controlled and similar mechanical stiffness, alongside tuned electrical conductivity, ranging from less to more conductive. These conditions enabled us to conduct well-tuned biological studies aimed at understanding how electrically conductive nanomaterials within hydrogel scaffolds (G-GNR) impact the functionalities and fate of cardiac tissues.

SEM images revealed the porous structure of the photopolymerized nanoengineered scaffolds (Figure 2C). A closer examination of the pore walls of G-GNR and G-SNP hydrogels confirmed the successful dispersion of GNRs and SNPs within the pores of the hydrogel matrix, creating a conducive microenvironment for cell interaction with the nanoparticles (Figure 2C). This homogeneous distribution of nanoparticles within the hydrogel scaffolds was consistent with our previous studies with the use of GNRs dispersed within the GelMA hydrogel for studies involving NRVMs.[35,37] Energy-dispersive X-ray spectroscopy (EDS) was employed to further corroborate the presence of nanoparticles within the hydrogel scaffolds. As expected, the presence of gold (Au) and silicon (Si) was detected within the nanoengineered hydrogel scaffolds (Figure S3). Incorporating nanoparticles within the hydrogel scaffolds may result in structural changes, as well. While there was no difference in the porosity between GelMA (pristine) and G-GNR hydrogel scaffolds, the porosity of G-SNP was lower compared to that of G-GNR hydrogels (Figure S4C). This observation aligns with the previous reports, where the porosity of hydrogel nanocomposites decreased upon the addition of silica nanoparticles.[56] It is also speculated that the physical reinforcement of the hydrogel network by silica nanoparticles resulted in lower porosity compared to the GelMA and G-GNR scaffolds.[56] Additionally, potential differences in the surface charges of GNRs and SNPs could have led to varied electrostatic attraction forces, resulting in reduced porosity in the G-SNP group compared to the G-GNR group. We also tested if the changes in porosity could potentially impact other surface characteristics, such as surface roughness. However, the surface morphology of the hydrogel scaffolds did not appear to vary significantly across different hydrogels, as assessed by optical coherence tomography (OCT) imaging (Figure S4A,B).

3.2. Assessment of Cardiac Tissue Formation on the Nanoengineered Hydrogel Scaffolds. Initially, hiCMs and hiCFs were cocultured on the hydrogel scaffolds to assess the biocompatibility of the substrates. The live/dead assay confirmed no significant cell death across the hydrogel groups (Figure S5A,B), consistent with the previous reports.[35,38,55] Additionally, higher doses of the nanoparticles were tested to assess the viability of the cardiac cells. While there were no significant differences among the GelMA, G-GNR (1.0 mg/mL), and G-SNP (1.4 mg/mL) groups, higher concentration of GNRs and SNPs led to significantly lower viability compared to the GelMA group (control) as demonstrated in Figure S6. Upon formation, cardiac tissues were cultured for 14 days, and phase contrast images were captured on days 1, 3, 7, and 14 (Figure S7). On days 1 and 3, the phase contrast images demonstrated uniform cell attachment on the hydrogel surfaces. Notably, spontaneous beating of cardiac tissues was observed around day 3 of the culture across all experimental groups.

Given the surface chemical differences between GNRs and SNPs, which might lead to varying structural changes in GelMA hydrogels, we investigated whether this resulted in any disparities in terms of cell attachment and cardiac tissue formation when cells are cultured atop hydrogel scaffolds. First, cardiac tissues were stained with F-actin and integrin β-1 to assess the phenotype of cardiac tissues formed on the nanoengineered hydrogel scaffolds. The IF-stained samples captured using a 20× objective displayed the robust formation of cardiac tissues across all the hydrogel groups (Figure S8). Additionally, the cardiac tissues formed on 2D Matrigel-coated standard well plates were also stained for F-actin and Integrin as

https://doi.org/10.1021/acsbiomaterials.3c01256
ACS Biomater. Sci. Eng. 2024, 10, 2351−2366

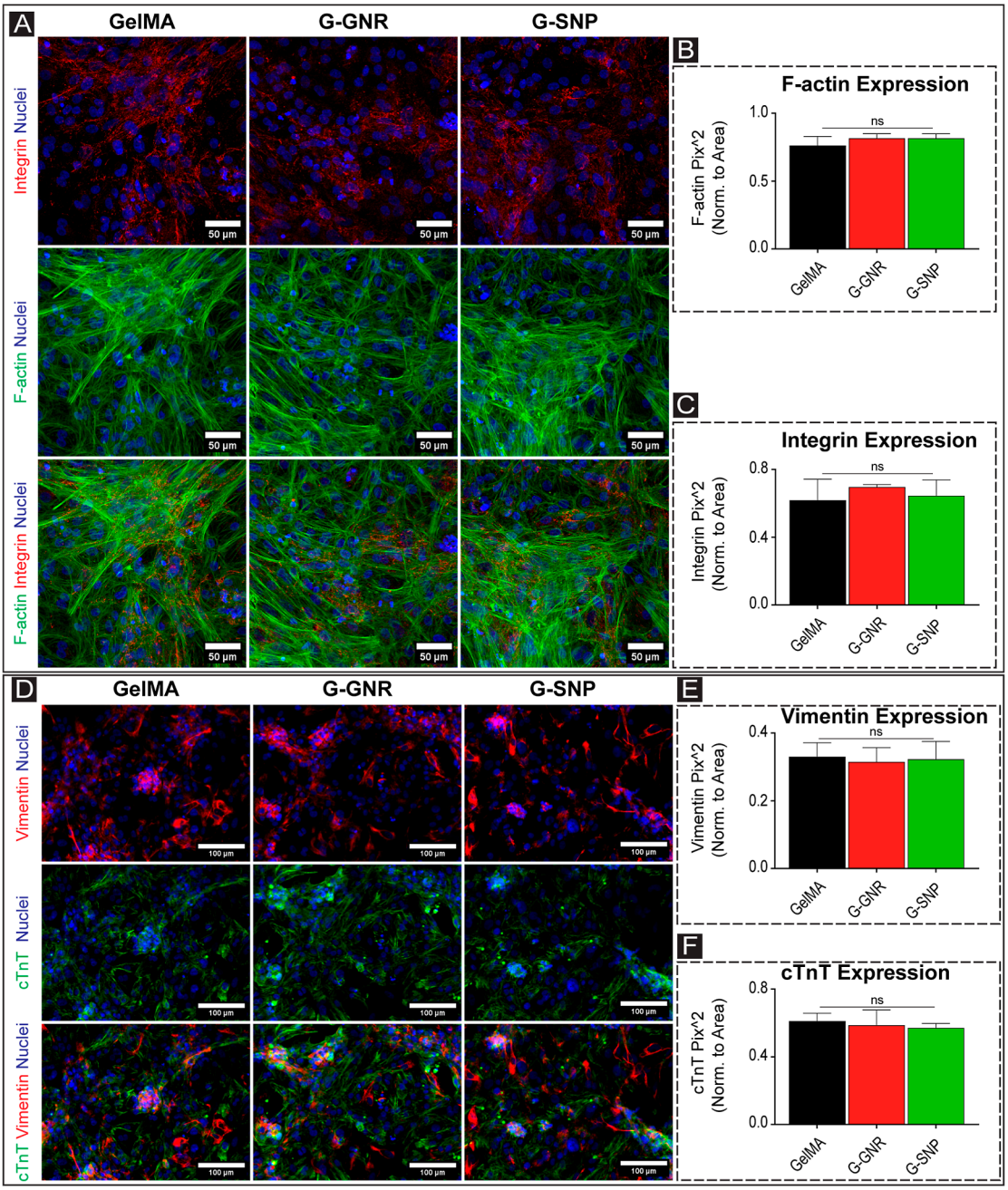

Figure 3. Phenotype of cardiac tissues grown on nanoengineered hydrogel scaffolds. (A) Immunofluorescence (IF) images of cardiac tissues formed on GelMA, G-GNR, and G-SNP hydrogel scaffolds for 14 days stained for integrin (red), F-actin (green), and nuclei (blue). Scale bar: 50 μm. Cell coverage analysis of the cardiac tissues formed on the nanoengineered hydrogel scaffolds measured by F-actin (B) and Integrin β1 (C) (one-way ANOVA with a Tukey's posthoc test, $n = 3$). (D) IF images of cardiac tissues stained for vimentin (red), cardiac troponin T (cTnT) (green), and nuclei (blue). Scale bar: 100 μm. (E) The level of vimentin expression and (F) cTnT expression of the cardiac tissues formed on the nanoengineered hydrogel scaffolds measured by ImageJ (one-way ANOVA with a Tukey's posthoc test, $n = 3$). Data were expressed as mean ± standard deviation. ns (not significant).

a control to assess the overall morphology of the cardiac tissues formed on the nanoengineered hydrogel scaffolds. The IF images showed that cardiac tissues formed on hydrogel scaffolds had a similar morphology compared with those cultured on 2D Matrigel-coated well plates (Figure S9A). For a more detailed examination of the cardiac tissues, samples were also imaged at 40× magnification (Figure 3A). A prior study involving NRVMs reported enhanced cell attachment and coverage on hydrogel scaffolds incorporated with GNRs.[35] However, the cell coverage measured by F-actin expression and the cell−matrix interaction quantified by integrin β-1 expression were not significantly different within the nanoengineered hydrogel scaffolds when compared to the pristine GelMA group (Figure 3B,C). This finding suggests that the addition of nanoparticles (GNRs and SNPs) did not adversely impact cardiac cell attachment.

Next, we investigated the distribution and organization of hiCMs and hiCFs within cardiac tissues. To achieve this, we performed IF staining for cTnT and vimentin markers, which are specific to hiCMs and hiCFs, respectively (Figure 3D). Quantification analysis of the vimentin and cTnT positive

https://doi.org/10.1021/acsbiomaterials.3c01256
ACS Biomater. Sci. Eng. 2024, 10, 2351−2366

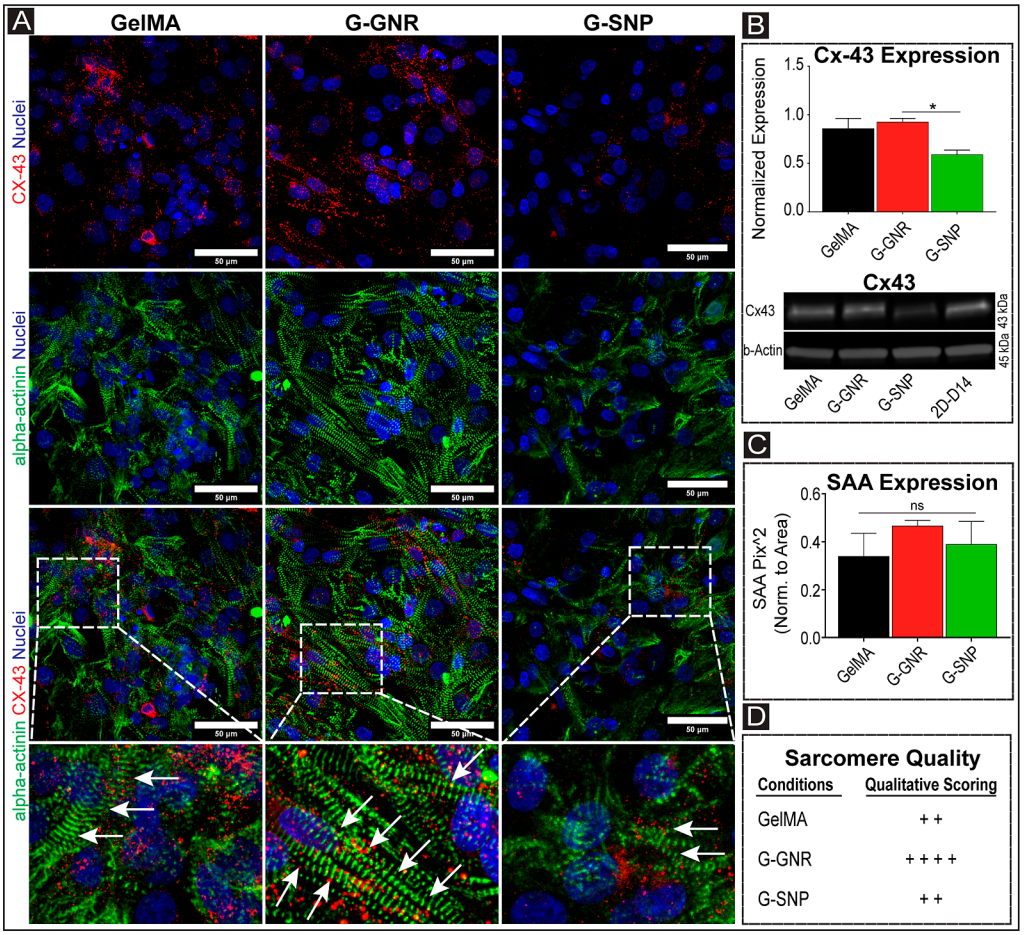

Figure 4. Phenotype evaluation of cardiac tissues formed on the nanoengineered scaffolds using the expression of cardiac-specific markers. (A) IF images of cardiac tissues formed on GelMA, G-GNR, and G-SNP hydrogel scaffolds for 14 days stained for alpha-actinin (green), Cx43 (red), and nuclei (blue). Scale bar: 50 μm. Magnified images are shown at the bottom with white arrows indicating the organized and striated patterns of the sarcomere structure. (B) Relative expression of Cx43 in the cardiac tissues formed on GelMA, G-GNR, and G-SNP measured by Western blot (one-way ANOVA with a Tukey's posthoc test, $n = 2$). Data were expressed as mean ± standard deviation. *$p < 0.05$, and ns (not significant). (C) Relative expression of alpha-actinin in the cardiac tissues formed on GelMA, G-GNR, and G-SNP measured by ImageJ using alpha-actinin stained images (one-way ANOVA with a Tukey's posthoc test, $n = 3$). (D) Qualitative scoring of sarcomere quality showing the highest quality of the sarcomere structure of the cardiac tissues formed on the G-GNR scaffolds.

areas confirmed no significant difference among the conditions, particularly between the conductive and nonconductive groups (Figure 3E,F). This finding and confirmation was particularly important as disparities in cell number and type between the G-GNR and G-SNP groups after the 14 day culture period could potentially impact further downstream assay analysis. Overall, the IF imaging of the cardiac tissues formed on the nanoengineered hydrogel scaffolds led to the conclusion that SNP serves as a suitable nonconductive control group for GNRs.

3.3. Expression of Cardiac-Specific Proteins on the Nanoengineered Hydrogel Scaffolds. The cardiac tissue phenotype was further analyzed through IF staining of the samples using cardiac-specific markers, namely, Cx43, a gap-junction protein mediating the electrical coupling of cardiac cells,[57] and SAA, a sarcomeric protein localized at the *Z*-disks.[58] As exhibited in the IF-stained images of Cx43 (Figure 4A, top row), Western blot analysis also demonstrated a significant reduction in Cx43 expression in the G-SNP group compared to that in the G-GNR group (Figure 4B). We speculate that the nonconductive substrate (G-SNP) led to nanoscale insulating regions within the matrix, contributing to reduced crosstalk among cardiac cells and subsequently decreasing the expression of the gap junction protein Cx43 expression. This finding corresponds with a previous study where conductive hydrogel scaffolds, created by incorporating gold nanospheres, resulted in enhanced Cx43 expression in cultured rat-derived cardiac cells compared to nonconductive scaffolds (control group).[59] Furthermore, IF images confirmed the expression and organization of striated SAA and Cx43 proteins in hiCMs cultured on G-GNR hydrogel as well as on pristine GelMA and nonconductive G-SNP hydrogels. While the SAA protein expression did not exhibit a significant difference among the experimental conditions (Figure 4C), higher magnification confocal images, along with qualitative scoring, revealed a more organized and directional striation of sarcomeres (indicated by white arrows) on the electrically conductive G-GNR hydrogels (Figures 4A,D and S10). This observation aligns with previous studies where the incorporation of reduced graphene oxide[60] and gold nanoparticles[55,61] into hydrogel scaffolds promoted the formation of striated cardiac tissues.

3.4. Gene Expression Analysis. To delve deeper into the molecular-level interaction of hiPSCs-CMs with nanoengineered hydrogels, gene expression analysis was conducted on a panel of cardiac-specific genes. Specifically, we assessed the

https://doi.org/10.1021/acsbiomaterials.3c01256
ACS Biomater. Sci. Eng. 2024, 10, 2351−2366

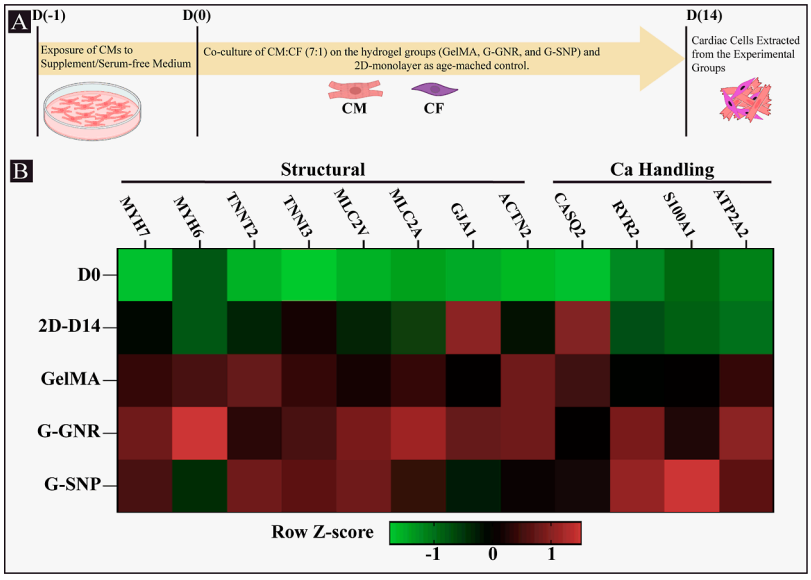

Figure 5. Gene expression analysis of the cardiac tissues formed on the nanoengineered scaffolds. (A) Schematic outline of the gene expression study workflow. hiCMs were exposed to a supplement-free medium for 24 h before culture on the condition groups. hiCMs and hiCFs with the 7:1 ratio was cocultured on hydrogel scaffolds for 14 days before sample collection and lysing for gene expression analysis. As a control for gene expression normalization, a portion of hiCMs and hiCFs with the same 7:1 ratio was lysed at day 0 before culturing on the scaffolds. (B) The heatmap showing the expression fold changes of structural and calcium handling genes across the culture conditions with *z*-score displayed ($n = 3$). The heatmap represents the expression of the cardiac structural genes (ACTN2, GJA1, MLC2A, MLC2 V, TNNI3, TNNT2, MYH6, and MYH7) and calcium handling genes (ATP2A2, S100A1, RYR2, and CASQ2) in cardiac tissues formed on GelMA, G-GNR, and G-SNP for 14 days compared to aged-matched 2D monolayer condition (2D-D14) and the day 0 cardiac cell population ($n = 3$).

expression of genes related to the ultrastructure (ACTN2, GJA1, MLC2A, MLC2 V, TNNI3, TNNT2, MYH6, and MYH7) and calcium handling (ATP2A2, S100A1, RYR2, and CASQ2).[62] Prior to cell culture on the hydrogel scaffolds, the cell cycle of differentiated hiCMs was synchronized by maintaining them in the supplement/serum-free medium for 24 h.[63] The 14-day-old cardiac tissues formed on the hydrogel scaffolds (GelMA, G-GNR, and G-SNP) and an age-matched 2D monolayer control (2D-D14) were compared to a mixture of cells containing the same 7:1 ratio of hiCMs and hiCFs prior to seeding atop the hydrogel matrices (termed D0; Figure 5A). The expression of each gene was compared across the experimental groups, specifically between electrically conductive and nonconductive nanoengineered hydrogels. The *z*-score derived from the average fold changes of the tissues extracted from the hydrogels, 2D-D14, and day 0 groups were plotted in a heatmap (Figure 5B). Based on the heatmap (where red color indicates upregulation and green color indicates downregulation), while not significantly different, compared to the cell population at day 0 and the 2D-D14 condition, the expression level of cardiac genes such as MYH7, TNNT2, TNNI3, and ATP2A2 was enhanced in the cardiac tissues formed on the hydrogel scaffold groups. Specifically, the expression of calcium handling genes, including ATP2A2 (ATPase Sarcoplasmic Reticulum Ca^{2+} Transporting 2), which encodes SERCA2 to maintain the cytosolic calcium homeostasis[62] and RYR2 (ryanodine receptor), which is involved in hiCM contractility, showed increased expression in G-GNR and G-SNP conditions. Additionally, MLC2 V, a sarcomere-related gene, had enhanced expression in the G-GNR and G-SNP conditions. Comparatively, ACTNT2, a sarcomere-related gene in the adult heart,[64] exhibited a less pronounced expression in the nonconductive G-SNP group as compared to the GelMA and G-GNR groups.

The TNNI3 gene (encodes for cardiac troponin I), an essential component of the contractile machinery in adult CMs,[62] exhibited an increased expression trend in the G-GNR and G-SNP conditions. Thus, the increased expression of this gene in the G-GNR and G-SNP conditions further sheds light on potential improvement in the differentiation of cardiac tissues.

Considering the Western blot data discussed earlier, the significantly lower expression of the Cx43 protein in the G-SNP group compared to the G-GNR group aligned with the expression trend of the encoding gene for Cx43 (GJA1). This provides further support for the influence of conductivity on gap junction formation within cardiac tissues and its potential role in promoting cardiac tissue function and structure. A similar trend was observed in a recent study where genes associated with calcium handling (ATP2A2) and sarcomere (MYH7) genes were upregulated in cardiac tissues cultured on electrically conductive hydrogels generated by embedding reduced graphene oxide in decellularized porcine myocardial extracellular matrix.[60]

Interestingly, the GJA1 expression level in 2D-D14 condition exhibited a slight enhancement and was comparable to that of the cardiac tissues in the G-GNR (conductive) scaffolds. The GJA1 gene, which encodes the structural protein Cx43, has been demonstrated to be expressed between hiCF:hiCF in addition to hiCF:hiCM junctions.[65] Therefore, in addition to the interactions of hiCMs with each other, the interaction of hiCFs with hiCFs and hiCMs could also impact the expression level of this gene. Furthermore, in our study, while the culture conditions were similar among the hydrogel scaffolds, within the Matrigel-coated 2D culture system, the stiffness of plastic culture substrate could have influenced the cellular interactions and subsequently GJA1 gene expression. The enhanced expression level of GJA1 in the 2D monolayer system has also been

https://doi.org/10.1021/acsbiomaterials.3c01256
ACS Biomater. Sci. Eng. 2024, 10, 2351−2366

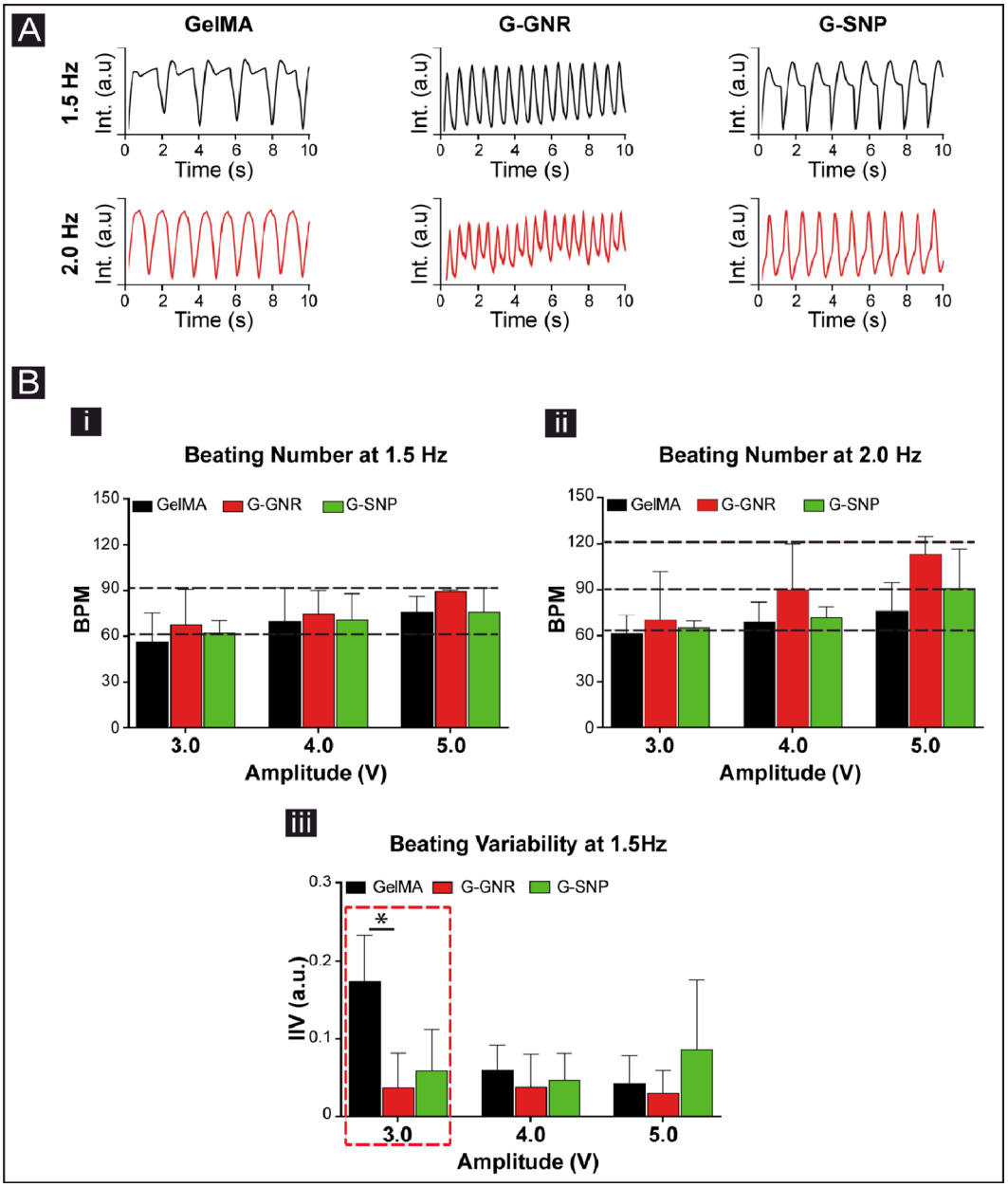

Figure 6. Beating behavior of stimulated cardiac tissues formed on the nanoengineered hydrogel scaffolds. (A) Representative beating signal graphs of cardiac tissues formed on GelMA, G-GNR, and G-SNP stimulated at various frequencies and 3.0 V. (B) Beating frequencies at 1.5 (i) and 2.0 Hz (ii), and interbeat interval variability (IIV) (iii) data extracted from beating signals of cardiac tissues formed on the nanoengineered hydrogel scaffolds at day 14 under various frequencies and amplitudes (one-way ANOVA with a Tukey's posthoc test, $n = 3$). Data were expressed as mean ± standard deviation. $^*p < 0.05$.

previously reported by Veldhuizen et al.,[42] as compared to the hydrogel groups.

MYH6 and MYH7 are both sarcomeric-related genes that are expressed during heart development with varying expression levels. MYH6 associated with early fetal stage, while MYH7 becomes more pronounced during the late stage of heart development.[66] In our study, while both genes showed enhanced expression, MYH6 was upregulated to a higher extent compared to MYH7 in the G- GNR group. Overall, despite improved gene expression in the cardiac tissues formed in hydrogel scaffolds compared to day 0 and 2D-D14 culture conditions, cardiac tissues may have still remained in a developmentally immature state as compared to the adult stage. This observation aligns with previous reports where the most differentiated *in vitro* hiPSC-derived cardiac population remained more developmentally immature than even the first trimester human hearts.[67]

3.5. Electrophysiological Analysis. To explore the impact of hydrogel scaffolds, specifically nanoengineered ones, on cardiac tissue-level function, we assessed the electrophysiological behavior of the cardiac tissues, such as interbeat interval variability (IIV), beats per minute (BPM), and beating patterns under different conditions. Initially, we analyzed the spontaneous beating signals of the tissues from real-time videos on days 3, 7, and 14 of culture (Figure S11). The beating signals exhibited a consistent pattern across all hydrogel conditions at all time points with similar contraction and relaxation patterns (Figure S11A). While the BPM generally increased to around 80

https://doi.org/10.1021/acsbiomaterials.3c01256
ACS Biomater. Sci. Eng. 2024, 10, 2351−2366

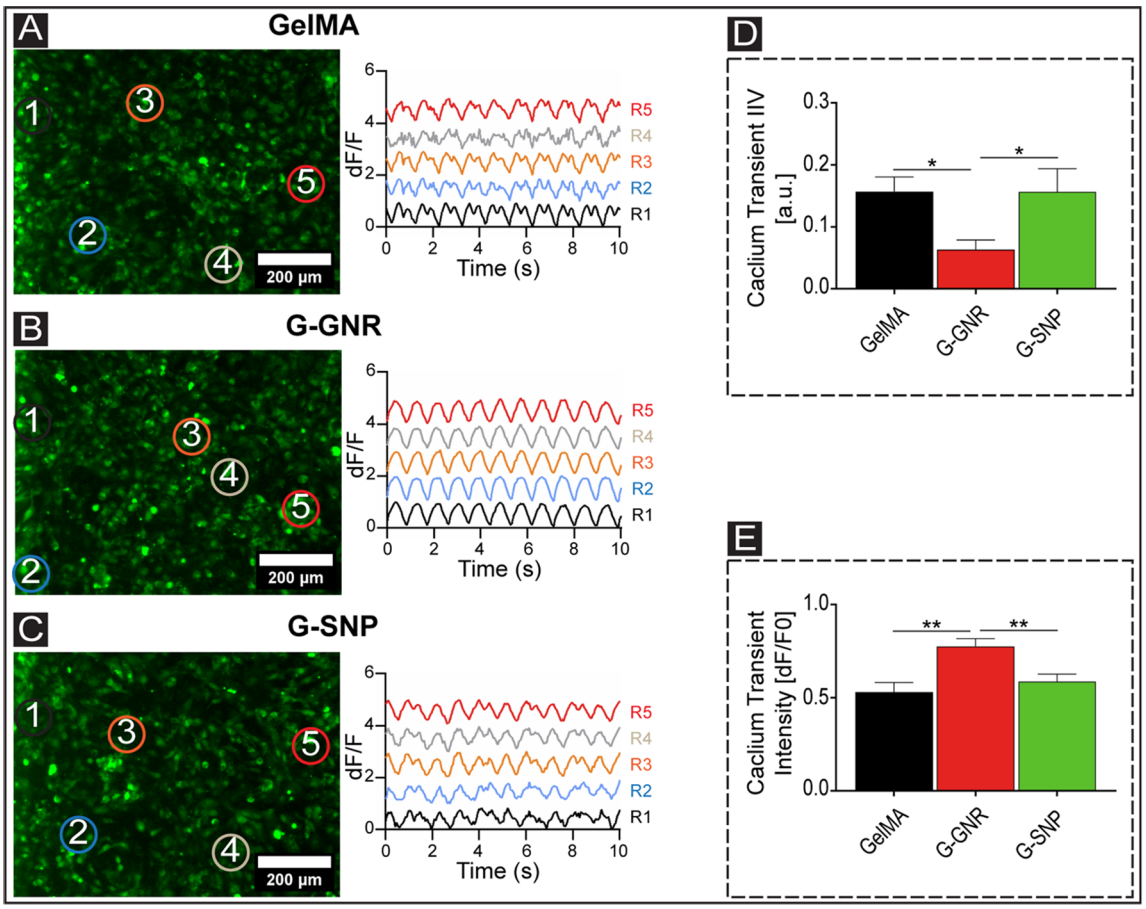

Figure 7. Ca transient analysis of the cardiac tissues formed on the nanoengineered scaffolds. Calcium transient signals for the cardiac tissues formed on GelMA (A), G-GNR (B), and G-SNP (C) were measured under 1.0 Hz stimulation. Five regions were selected per image and the correlated signals of each region were shown on the graphs. Scale bar: 200 μm. (D) Interbeat interval variability (IIV) data extracted from calcium spikes of cardiac tissues formed on the nanoengineered hydrogel scaffolds at day 14 of culture (one-way ANOVA with a Tukey's posthoc test, $n = 3$). (E) Calcium transient intensity data extracted from calcium spikes of cardiac tissues formed on the nanoengineered hydrogel scaffolds at day 14 of culture (one-way ANOVA with a Tukey's posthoc test, $n = 3$). Data were expressed as mean ± standard deviation. *$p < 0.05$, **$p < 0.01$, and ns (not significant).

at D14 compared to approximately 55 at days 3 and 7, there were no significant differences in BPM values among the conditions at each time point (Figure S11B). Additionally, we quantified IIV to evaluate the synchronicity of beating tissues on each scaffold, yet no significant differences were observed among the conditions (Figure S11C).

Given the absence of significant differences in spontaneous beating characteristics, we aimed to determine if cardiac tissues formed on conductive and nonconductive scaffolds respond differently to external electrical stimulation. For this purpose, a custom-made electrical stimulation platform was developed,[51] and the 14-day-old cardiac tissues were placed between carbon electrodes in the presence of the cell culture medium (RPMI/B27 with insulin). The cardiac tissues were paced at frequencies of 1.0, 1.5, and 2.0 Hz, with amplitudes ranging from 1.0 to a maximum of 10.0 V in a 1.0 V increment. Due to the spontaneous beating of the cardiac tissues around 1.0 Hz (60 BPM), it was not possible to discern changes in beating rate at various amplitudes. Therefore, data acquired from the stimulations at 1.5 and 2.0 Hz were used for further analysis and comparison among experimental groups. The cardiac tissues formed on G-GNR hydrogel scaffolds exhibited a different beating pattern as they adapted their beating to the applied frequencies (1.5 and 2.0 Hz) (Figure 6A). Quantitative analysis of the cardiac tissues (Figure 6B(i,ii)) demonstrated that, at the higher external applied voltage (i.e., 5 V), electrically conductive G-GNR tissues better synchronized with the pacing (Videos S1 and S2). This adaptation could result from the enhanced functionality of cardiac tissues developed on the G-GNR substrate, attributed to improved cell−cell communication and the facilitation of electrical signal propagation across the cardiac tissue. To further assess tissue synchronicity using IIV, cardiac tissues paced at 3.0, 4.0, and 5.0 V and 1.5 Hz were analyzed, as this was the range at which the tissues began responding to the stimulation regime. IIV was found to be significantly reduced in the G-GNR condition at 3.0 V compared to the pure GelMA group (Figure 6B(iii)), while the IIV was not significantly different compared to the other conditions at 4.0 and 5.0 V.

To further assess the functionality of the cardiac tissues, we recorded calcium transient videos and quantitatively analyzed them for the cardiac tissues formed over 14 days on the hydrogel scaffolds. To ensure consistency among the conditions, the cardiac tissues were paced at 1.0 Hz and calcium transients from at least three regions of interest (ROI) were recorded for each group. The cardiac tissues formed on GelMA, and G-SNP exhibited asynchronous calcium flux peaks at different subregions (Figure 7A,C,D and Video S3). In contrast, synchronous calcium flux patterns were observed in the subregions of cardiac tissues formed on G-GNR (Figure 7B,D and Video S3). Furthermore, the calcium transient intensity was

https://doi.org/10.1021/acsbiomaterials.3c01256
ACS Biomater. Sci. Eng. 2024, 10, 2351−2366

significantly higher in cardiac tissues formed on the G-GNR substrates than that in the GelMA and G-SNP groups (Figure 7E). This indicates that the hiCMs cultured and grown on the G-GNR scaffolds were successfully coupled resulting in improved calcium handling properties. Furthermore, the embedded GNR within the GelMA hydrogel scaffolds bridged nonconductive regions of the scaffold, leading to synchronous calcium release within the regions of interest, which is consistent with previously reported studies.[35] In addition, among the hydrogel scaffold groups, gene expression analysis (Figure 5B) indicated that GJA1 expression was increased only in the G-GNR group. This increase might have facilitated the signal propagation within the cardiac tissues formed in the G-GNR condition, aligning with tissue-level enhanced function indicated by the calcium transients.

In this study, the impact of nanoengineered electrically conductive and nonconductive hydrogels on the functionality of cardiac tissues, seeded with hiCMs in coculture with hiCFs, was assessed simultaneously. Compared to the nonconductive hydrogel scaffold (G-SNP), enhancements in SAA striation, Cx43 expression, and calcium transients were observed in cardiac tissues formed on electrically conductive G-GNR hydrogels. This suggests a positive influence of the electroconductivity features of GNRs on the functionalities and cross-talk among cardiac cells. However, the gene expression profile was not statistically different in cardiac tissues grown on both electrically conductive G-GNR and nonconductive G-SNP groups.

Although we primarily focused on the contribution of conductive features of GNRs on cardiac tissue function, structure, and morphology (i.e., Sarcomere organization, calcium transients), GNRs can also introduce other features to the hydrogel scaffolds used for cardiac tissue engineering. For instance, the increased localized stiffness of collagen-based hydrogels imparted by GNRs was previously shown[39] to advance the differentiation of neonatal rat derived cardiac tissues toward the adult-stage via β1 integrin-mediated integrin-linked kinase (ILK)/phosphorylated serine−threonine kinase (p-AKT)/GATA4 signaling pathway. In our study, while the bulk stiffness was maintained the same across the hydrogel scaffolds, the addition of GNRs and SNPs could have modulated the nanoscale localized stiffness of the hydrogel scaffolds. The assessment of the effect of the localized stiffnesses of these GNR-based electroconductive and nonconductive hydrogel scaffolds will be the focus of our future studies, potentially unveiling the underlying synergistic mechanisms that enhance the functionality of cardiac tissues formed atop nanoengineered hydrogel matrices.

It is worth noting that 2D cell-seeded hydrogel systems, as employed in our study, are crucial and informative for assessing the overall influence of nanoparticles on cardiac tissues for applications in drug screening, regenerative medicine, and mechanistic studies. However, it is acknowledged that 2D hydrogel-based culture systems may not fully replicate the complexity of the *in vivo* cardiac tissue microenvironment. Recently, the 3D encapsulation of hiPSC-CMs in hydrogel scaffolds embedded with gold nanospheres has been shown to enhance the functionality of cardiac tissues.[61] Further 3D studies with various types of gold nanoparticles, such as GNRs and gold nanowires, are imperative to fully assess the cardiac cell function in response to nanoparticles within a more *in vivo* like microenvironment, which is the subject of our current ongoing studies.

Overall, we demonstrated the successful integration of gold and silica nanoparticles into hydrogel scaffolds, supporting the formation and function of human cardiac tissues in a 2D cell-seeded hydrogel-based culture system. The emergence of more sophisticated fabrication strategies such as 3D bioprinting may also present a promising approach for the development of biomimetic cardiac tissue constructs, resembling *in vivo* condition. To that end, gold nanoparticles have been successfully incorporated into gelatin-based bioinks for 3D bioprinting of cardiac tissues derived from rat cardiac cells.[38] Due to the biocompatibility of gold and silica nanoparticles and, importantly, their ease of functionalization, these nanomaterials could further be explored for the development of hybrid and advanced nanoengineered bioinks with specific chemical and physical features tailored for innovative approaches in cardiac tissue engineering.

4. CONCLUSIONS

In this study, we developed and characterized two classes of nanoengineered hydrogel scaffolds, namely, electrically conductive and nonconductive GelMA hydrogels, to comprehensively assess the functionality of engineered cardiac tissues formed through the coculture of hiCMs and hiCFs. Specifically, we utilized gold nanorods (GNRs) and nonconductive silica nanoparticles (SNPs) embedded within photo-cross-linkable GelMA hydrogel for our investigations. Our findings revealed that the sarcomere structure of the cardiac tissues formed atop of the G-GNR hydrogel was more organized and striated, indicating a positive influence of electrical conductivity features on the cardiac tissue phenotype. Interestingly, Western blot data indicated that Cx43 expression in the cardiac tissues grown on the hydrogel scaffold with the lowest conductivity (G-SNP, most insulating) was significantly lower than that under the G-GNR condition possessing the highest conductivity. However, the gene expression profile of cell seeded on the conductive (G-GNR) and nonconductive (G-SNP) nanoengineered hydrogels was similar. On the other hand, the calcium transient analysis demonstrated the significant influence of electrical conductivity of the hydrogel scaffolds on the tissue signal propagation, as calcium spikes of the cells seeded on the G-GNR group were more synchronized compared to other groups. While the electrically conductive GNRs led to enhanced functionalities and structure of the cardiac tissue to some degree, our findings based on gene expression analyses demonstrated that the electrical conductivity of nanomaterials may not be the sole factor influencing the function, fate, and the phenotype of hiPSC-derived cardiac tissues when the cells are seeded atop hydrogel matrices.

■ ASSOCIATED CONTENT

Data Availability Statement

The raw and processed data for the generation of the presented data are available upon request from authors.

Supporting Information

The Supporting Information is available free of charge at https://pubs.acs.org/doi/10.1021/acsbiomaterials.3c01256.

hiPSC-derived cardiac tissues under electrical stimulation at 3.0 V and 1.5 Hz (MP4)

hiPSC-derived cardiac tissues under electrical stimulation at 3.0 V and 2.0 Hz (MP4)

Calcium transient responses of hiPSC-derived cardiac tissues (MP4)

https://doi.org/10.1021/acsbiomaterials.3c01256
ACS Biomater. Sci. Eng. 2024, 10, 2351−2366

Schematic illustration of GNR synthesis, size measurement analysis of GNRs, EDS analysis of nanoparticle-incorporated scaffolds, surface topography analysis of scaffolds, viability analysis of hydrogel scaffolds, viability analysis of hydrogel scaffolds at high concentrations of nanoparticles, phase contrast images of cardiac tissues, integrin- and F-actin-stained images of cardiac tissues, IF-stained images of cardiac tissues in 2D tissue culture plate, IF-stained images of cardiac tissues with cardiac-specific markers, spontaneous beating analysis of cardiac tissues, list of the used reagents, and list of the used primers (PDF)

AUTHOR INFORMATION

Corresponding Author

Mehdi Nikkhah − *School of Biological and Health Systems Engineering, Arizona State University, Tempe, Arizona 85287, United States; Biodesign Virginia G. Piper Center for Personalized Diagnosis, Arizona State University, Tempe, Arizona 85287, United States;* orcid.org/0000-0001-5970-7666; Email: Mehdi.Nikkhah@asu.edu

Authors

Hamid Esmaeili − *School of Biological and Health Systems Engineering, Arizona State University, Tempe, Arizona 85287, United States;* orcid.org/0000-0001-8003-8153

Alejandra Patino-Guerrero − *School of Biological and Health Systems Engineering, Arizona State University, Tempe, Arizona 85287, United States; Department of Cardiovascular Diseases, Physiology and Biomedical Engineering, Center for Regenerative Medicine, Mayo Clinic, Scottsdale, Arizona 85259, United States;* orcid.org/0000-0003-1223-6558

Ronald A. Nelson, Jr. − *School of Biological and Health Systems Engineering, Arizona State University, Tempe, Arizona 85287, United States*

Nina Karamanova − *Phoenix Veterans Affairs Health Care System, Phoenix, Arizona 85022, United States*

Taylor M. Fisher − *School of Sustainable Engineering and the Built Environment, Arizona State University, Tempe, Arizona 85287, United States*

Wuqiang Zhu − *Department of Cardiovascular Diseases, Physiology and Biomedical Engineering, Center for Regenerative Medicine, Mayo Clinic, Scottsdale, Arizona 85259, United States;* orcid.org/0000-0001-5217-7789

François Perreault − *School of Sustainable Engineering and the Built Environment, Arizona State University, Tempe, Arizona 85287, United States;* orcid.org/0000-0002-4756-8205

Raymond Q. Migrino − *Phoenix Veterans Affairs Health Care System, Phoenix, Arizona 85022, United States; University of Arizona College of Medicine, Phoenix, Arizona 85004, United States*

Complete contact information is available at: https://pubs.acs.org/10.1021/acsbiomaterials.3c01256

Author Contributions

Hamid Esmaeili: conceptualization, methodology, validation, formal analysis, investigation, data curation, writing—original draft, writing—review and editing, and visualization. **Alejandra Patino-Guerrero**: formal analysis. **Ronald A Nelson Jr.**: formal Analysis. **Nina Karamanova**: formal analysis. **Taylor Mackenzie Fisher**: formal analysis. **Wuqiang Zhu**: writing—review and editing. **François Perreault**: resources and writing—review and editing. **Raymond Q. Migrino**: conceptualization and writing—review and editing. **Mehdi Nikkhah**: conceptualization, methodology, resources, writing—review and editing, supervision, project administration, and funding acquisition.

Notes

The authors declare no competing financial interest.

ACKNOWLEDGMENTS

The authors would like to thank National Science Foundation (NSF) Award #2016501 for financially supporting this project. The authors would also like to acknowledge Prof. Paul Westerhoff for his scientific input on the project, Prof. Barbara Smith for providing qTower 2.0 access for qPCR analysis, Prof. Juliann Holloway for assisting in compressive modulus measurement, and Prof. Jennifer Christen for providing us with the EIS setup for Impedance measurement.

REFERENCES

(1) Mozaffarian, D.; Benjamin, E. J.; Go, A. S.; Arnett, D. K.; Blaha, M. J.; Cushman, M.; Das, S. R.; De Ferranti, S.; Després, J. P.; Fullerton, H. J.; et al. Heart disease and stroke statistics—2016 update: a report from the American Heart Association. *Circulation* **2016**, *133* (4), e38−e360.

(2) Murry, C. E.; Reinecke, H.; Pabon, L. M. Regeneration gaps: observations on stem cells and cardiac repair. *J. Am. Coll. Cardiol.* **2006**, *47* (9), 1777−1785.

(3) Bergmann, O.; Bhardwaj, R. D.; Bernard, S.; Zdunek, S.; Barnabé-Heider, F.; Walsh, S.; Zupicich, J.; Alkass, K.; Buchholz, B. A.; Druid, H.; et al. Evidence for cardiomyocyte renewal in humans. *Science* **2009**, *324* (5923), 98−102.

(4) Gourdie, R. G.; Dimmeler, S.; Kohl, P. Novel therapeutic strategies targeting fibroblasts and fibrosis in heart disease. *Nat. Rev. Drug Discovery* **2016**, *15* (9), 620−638.

(5) Ripplinger, C. M.; Lou, Q.; Li, W.; Hadley, J.; Efimov, I. R. Panoramic imaging reveals basic mechanisms of induction and termination of ventricular tachycardia in rabbit heart with chronic infarction: implications for low-voltage cardioversion. *Heart Rhythm.* **2009**, *6* (1), 87−97.

(6) Liew, L. C.; Ho, B. X.; Soh, B.-S. Mending a broken heart: current strategies and limitations of cell-based therapy. *Stem Cell Res. Ther.* **2020**, *11* (1), 138.

(7) Patino-Guerrero, A.; Veldhuizen, J.; Zhu, W.; Migrino, R. Q.; Nikkhah, M. Three-dimensional scaffold-free microtissues engineered for cardiac repair. *J. Mater. Chem. B* **2020**, *8* (34), 7571−7590.

(8) Veldhuizen, J.; Migrino, R. Q.; Nikkhah, M. Three-dimensional microengineered models of human cardiac diseases. *J. Biol. Eng.* **2019**, *13* (1), 29.

(9) Cambria, E.; Pasqualini, F. S.; Wolint, P.; Günter, J.; Steiger, J.; Bopp, A.; Hoerstrup, S. P.; Emmert, M. Y. Translational cardiac stem cell therapy: advancing from first-generation to next-generation cell types. *npj Regener. Med.* **2017**, *2* (1), 17.

(10) Lian, X.; Hsiao, C.; Wilson, G.; Zhu, K.; Hazeltine, L. B.; Azarin, S. M.; Raval, K. K.; Zhang, J.; Kamp, T. J.; Palecek, S. P. Robust cardiomyocyte differentiation from human pluripotent stem cells via temporal modulation of canonical Wnt signaling. *Proc. Natl. Acad. Sci. U.S.A.* **2012**, *109* (27), E1848−E1857.

(11) Chong, J. J.; Yang, X.; Don, C. W.; Minami, E.; Liu, Y.-W.; Weyers, J. J.; Mahoney, W. M.; Van Biber, B.; Cook, S. M.; Palpant, N. J.; et al. Human embryonic-stem-cell-derived cardiomyocytes regenerate non-human primate hearts. *Nature* **2014**, *510* (7504), 273−277.

(12) Shiba, Y.; Gomibuchi, T.; Seto, T.; Wada, Y.; Ichimura, H.; Tanaka, Y.; Ogasawara, T.; Okada, K.; Shiba, N.; Sakamoto, K.; et al. Allogeneic transplantation of iPS cell-derived cardiomyocytes regenerates primate hearts. *Nature* **2016**, *538* (7625), 388−391.

(13) Yanamandala, M.; Zhu, W.; Garry, D. J.; Kamp, T. J.; Hare, J. M.; Jun, H.-w.; Yoon, Y.-s.; Bursac, N.; Prabhu, S. D.; Dorn, G. W.; et al. Overcoming the roadblocks to cardiac cell therapy using tissue engineering. *J. Am. Coll. Cardiol.* **2017**, *70* (6), 766−775.

(14) Talebian, S.; Mehrali, M.; Taebnia, N.; Pennisi, C. P.; Kadumudi, F. B.; Foroughi, J.; Hasany, M.; Nikkhah, M.; Akbari, M.; Orive, G.; et al. Self-healing hydrogels: The next paradigm shift in tissue engineering? *Advanced Science* **2019**, *6* (16), 1801664.
(15) Williams, C.; Budina, E.; Stoppel, W. L.; Sullivan, K. E.; Emani, S.; Emani, S. M.; Black, L. D., III Cardiac extracellular matrix-fibrin hybrid scaffolds with tunable properties for cardiovascular tissue engineering. *Acta Biomater.* **2015**, *14*, 84−95.
(16) Christman, K. L.; Vardanian, A. J.; Fang, Q.; Sievers, R. E.; Fok, H. H.; Lee, R. J. Injectable fibrin scaffold improves cell transplant survival, reduces infarct expansion, and induces neovasculature formation in ischemic myocardium. *J. Am. Coll. Cardiol.* **2004**, *44* (3), 654−660.
(17) Rinkevich-Shop, S.; Landa-Rouben, N.; Epstein, F. H.; Holbova, R.; Feinberg, M. S.; Goitein, O.; Kushnir, T.; Konen, E.; Leor, J. Injectable collagen implant improves survival, cardiac remodeling, and function in the early period after myocarditis in rats. *J. Cardiovasc. Pharmacol. Ther.* **2014**, *19* (5), 470−480.
(18) Blackburn, N. J.; Sofrenovic, T.; Kuraitis, D.; Ahmadi, A.; McNeill, B.; Deng, C.; Rayner, K. J.; Zhong, Z.; Ruel, M.; Suuronen, E. J. Timing underpins the benefits associated with injectable collagen biomaterial therapy for the treatment of myocardial infarction. *Biomaterials* **2015**, *39*, 182−192.
(19) Hao, T.; Li, J.; Yao, F.; Dong, D.; Wang, Y.; Yang, B.; Wang, C. Injectable fullerenol/alginate hydrogel for suppression of oxidative stress damage in brown adipose-derived stem cells and cardiac repair. *ACS Nano* **2017**, *11* (6), 5474−5488.
(20) Deng, B.; Shen, L.; Wu, Y.; Shen, Y.; Ding, X.; Lu, S.; Jia, J.; Qian, J.; Ge, J. Delivery of alginate-chitosan hydrogel promotes endogenous repair and preserves cardiac function in rats with myocardial infarction. *J. Biomed. Mater. Res., Part A* **2015**, *103* (3), 907−918.
(21) Dobner, S.; Bezuidenhout, D.; Govender, P.; Zilla, P.; Davies, N. A synthetic non-degradable polyethylene glycol hydrogel retards adverse post-infarct left ventricular remodeling. *J. Card. Failure* **2009**, *15* (7), 629−636.
(22) Navaei, A.; Truong, D.; Heffernan, J.; Cutts, J.; Brafman, D.; Sirianni, R. W.; Vernon, B.; Nikkhah, M. PNIPAAm-based biohybrid injectable hydrogel for cardiac tissue engineering. *Acta Biomater.* **2016**, *32*, 10−23.
(23) Monteiro, L. M.; Vasques-Nóvoa, F.; Ferreira, L.; Pinto-do-Ó, P.; Nascimento, D. S. Restoring heart function and electrical integrity: closing the circuit. *npj Regener. Med.* **2017**, *2*, 9.
(24) He, S.; Wu, J.; Li, S.-H.; Wang, L.; Sun, Y.; Xie, J.; Ramnath, D.; Weisel, R. D.; Yau, T. M.; Sung, H.-W.; et al. The conductive function of biopolymer corrects myocardial scar conduction blockage and resynchronizes contraction to prevent heart failure. *Biomaterials* **2020**, *258*, 120285.
(25) Esmaeili, H.; Patino-Guerrero, A.; Hasany, M.; Ansari, M. O.; Memic, A.; Dolatshahi-Pirouz, A.; Nikkhah, M. Electroconductive biomaterials for cardiac tissue engineering. *Acta Biomater.* **2022**, *139*, 118−140.
(26) Lee, J.; Manoharan, V.; Cheung, L.; Lee, S.; Cha, B.-H.; Newman, P.; Farzad, R.; Mehrotra, S.; Zhang, K.; Khan, F.; et al. Nanoparticle-based hybrid scaffolds for deciphering the role of multimodal cues in cardiac tissue engineering. *ACS Nano* **2019**, *13* (11), 12525−12539.
(27) Shin, S. R.; Jung, S. M.; Zalabany, M.; Kim, K.; Zorlutuna, P.; Kim, S. . b.; Nikkhah, M.; Khabiry, M.; Azize, M.; Kong, J.; et al. Carbon-nanotube-embedded hydrogel sheets for engineering cardiac constructs and bioactuators. *ACS Nano* **2013**, *7* (3), 2369−2380.
(28) Shin, S. R.; Zihlmann, C.; Akbari, M.; Assawes, P.; Cheung, L.; Zhang, K.; Manoharan, V.; Zhang, Y. S.; Yüksekkaya, M.; Wan, K. . t.; et al. Reduced graphene oxide-gelMA hybrid hydrogels as scaffolds for cardiac tissue engineering. *Small* **2016**, *12* (27), 3677−3689.
(29) Shin, S. R.; Aghaei-Ghareh-Bolagh, B.; Gao, X.; Nikkhah, M.; Jung, S. M.; Dolatshahi-Pirouz, A.; Kim, S. B.; Kim, S. M.; Dokmeci, M. R.; Tang, X.; et al. Layer-by-layer assembly of 3D tissue constructs with functionalized graphene. *Adv. Funct. Mater.* **2014**, *24* (39), 6136−6144.
(30) Kharaziha, M.; Shin, S. R.; Nikkhah, M.; Topkaya, S. N.; Masoumi, N.; Annabi, N.; Dokmeci, M. R.; Khademhosseini, A. Tough and flexible CNT-polymeric hybrid scaffolds for engineering cardiac constructs. *Biomaterials* **2014**, *35* (26), 7346−7354.
(31) Hsiao, C.-W.; Bai, M.-Y.; Chang, Y.; Chung, M.-F.; Lee, T.-Y.; Wu, C.-T.; Maiti, B.; Liao, Z.-X.; Li, R.-K.; Sung, H.-W. Electrical coupling of isolated cardiomyocyte clusters grown on aligned conductive nanofibrous meshes for their synchronized beating. *Biomaterials* **2013**, *34* (4), 1063−1072.
(32) Cobley, C. M.; Chen, J.; Cho, E. C.; Wang, L. V.; Xia, Y. Gold nanostructures: a class of multifunctional materials for biomedical applications. *Chem. Soc. Rev.* **2011**, *40* (1), 44−56.
(33) Karperien, L.; Navaei, A.; Godau, B.; Dolatshahi-Pirouz, A.; Akbari, M.; Nikkhah, M. Nanoengineered biomaterials for cardiac regeneration. *Nanoengineered Biomaterials for Regenerative Medicine*; Elsevier, 2019; pp 95−124.
(34) Dvir, T.; Timko, B. P.; Brigham, M. D.; Naik, S. R.; Karajanagi, S. S.; Levy, O.; Jin, H.; Parker, K. K.; Langer, R.; Kohane, D. S. Nanowired three-dimensional cardiac patches. *Nat. Nanotechnol.* **2011**, *6* (11), 720−725.
(35) Navaei, A.; Saini, H.; Christenson, W.; Sullivan, R. T.; Ros, R.; Nikkhah, M. Gold nanorod-incorporated gelatin-based conductive hydrogels for engineering cardiac tissue constructs. *Acta Biomater.* **2016**, *41*, 133−146.
(36) Navaei, A.; Moore, N.; Sullivan, R. T.; Truong, D.; Migrino, R. Q.; Nikkhah, M. Electrically conductive hydrogel-based micro-topographies for the development of organized cardiac tissues. *RSC Adv.* **2017**, *7* (6), 3302−3312.
(37) Navaei, A.; Rahmani Eliato, K.; Ros, R.; Migrino, R. Q.; Willis, B. C.; Nikkhah, M. The influence of electrically conductive and non-conductive nanocomposite scaffolds on the maturation and excitability of engineered cardiac tissues. *Biomater. Sci.* **2019**, *7* (2), 585−595.
(38) Zhu, K.; Shin, S. R.; van Kempen, T.; Li, Y. C.; Ponraj, V.; Nasajpour, A.; Mandla, S.; Hu, N.; Liu, X.; Leijten, J.; et al. Gold nanocomposite bioink for printing 3D cardiac constructs. *Adv. Funct. Mater.* **2017**, *27* (12), 1605352.
(39) Li, Y.; Shi, X.; Tian, L.; Sun, H.; Wu, Y.; Li, X.; Li, J.; Wei, Y.; Han, X.; Zhang, J.; et al. AuNP−Collagen Matrix with Localized Stiffness for Cardiac-Tissue Engineering: Enhancing the Assembly of Intercalated Discs by β1-Integrin-Mediated Signaling. *Adv. Mater.* **2016**, *28* (46), 10230−10235.
(40) Nikoobakht, B.; El-Sayed, M. A. Preparation and growth mechanism of gold nanorods (NRs) using seed-mediated growth method. *Chem. Mater.* **2003**, *15* (10), 1957−1962.
(41) Loessner, D.; Meinert, C.; Kaemmerer, E.; Martine, L. C.; Yue, K.; Levett, P. A.; Klein, T. J.; Melchels, F. P.; Khademhosseini, A.; Hutmacher, D. W. Functionalization, preparation and use of cell-laden gelatin methacryloyl-based hydrogels as modular tissue culture platforms. *Nat. Protoc.* **2016**, *11* (4), 727−746.
(42) Veldhuizen, J.; Cutts, J.; Brafman, D. A.; Migrino, R. Q.; Nikkhah, M. Engineering anisotropic human stem cell-derived three-dimensional cardiac tissue on-a-chip. *Biomaterials* **2020**, *256*, 120195.
(43) Patino-Guerrero, A.; Ponce Wong, R. D.; Kodibagkar, V. D.; Zhu, W.; Migrino, R. Q.; Graudejus, O.; Nikkhah, M. Development and Characterization of Isogenic Cardiac Organoids from Human-Induced Pluripotent Stem Cells Under Supplement Starvation Regimen. *ACS Biomater. Sci. Eng.* **2022**, *9*, 944−958.
(44) Veldhuizen, J.; Mann, H. F.; Karamanova, N.; Van Horn, W. D.; Migrino, R. Q.; Brafman, D.; Nikkhah, M. Modeling long QT syndrome type 2 on-a-chip via in-depth assessment of isogenic gene-edited 3D cardiac tissues. *Sci. Adv.* **2022**, *8* (50), No. eabq6720.
(45) Tohyama, S.; Hattori, F.; Sano, M.; Hishiki, T.; Nagahata, Y.; Matsuura, T.; Hashimoto, H.; Suzuki, T.; Yamashita, H.; Satoh, Y.; et al. Distinct metabolic flow enables large-scale purification of mouse and human pluripotent stem cell-derived cardiomyocytes. *Cell Stem Cell* **2013**, *12* (1), 127−137.
(46) Zhang, J.; Tao, R.; Campbell, K. F.; Carvalho, J. L.; Ruiz, E. C.; Kim, G. C.; Schmuck, E. G.; Raval, A. N.; da Rocha, A. M.; Herron, T. J.; et al. Functional cardiac fibroblasts derived from human pluripotent stem cells via second heart field progenitors. *Nat. Commun.* **2019**, *10* (1), 2238.

https://doi.org/10.1021/acsbiomaterials.3c01256
ACS Biomater. Sci. Eng. 2024, 10, 2351−2366

(47) Richards, D. J.; Tan, Y.; Coyle, R.; Li, Y.; Xu, R.; Yeung, N.; Parker, A.; Menick, D. R.; Tian, B.; Mei, Y. Nanowires and electrical stimulation synergistically improve functions of hiPSC cardiac spheroids. *Nano Lett.* **2016**, *16* (7), 4670−4678.
(48) Benbuk, A. A.; Esmaeili, H.; Liu, S.; Patino-Guerrero, A.; Migrino, R. Q.; Chae, J.; Nikkhah, M.; Blain Christen, J. Passive and Flexible Wireless Electronics Fabricated on Parylene/PDMS Substrate for Stimulation of Human Stem Cell-Derived Cardiomyocytes. *ACS Sens.* **2022**, *7* (11), 3287−3297.
(49) Veldhuizen, J.; Chavan, R.; Moghadas, B.; Park, J. G.; Kodibagkar, V. D.; Migrino, R. Q.; Nikkhah, M. Cardiac ischemia on-a-chip to investigate cellular and molecular response of myocardial tissue under hypoxia. *Biomaterials* **2022**, *281*, 121336.
(50) Veldhuizen, J.; Nikkhah, M. Developing 3D organized human cardiac tissue within a microfluidic platform. *J. Visualized Exp.* **2021**, No. 172, No. e62539.
(51) Tandon, N.; Cannizzaro, C.; Chao, P.-H. G.; Maidhof, R.; Marsano, A.; Au, H. T. H.; Radisic, M.; Vunjak-Novakovic, G. Electrical stimulation systems for cardiac tissue engineering. *Nat. Protoc.* **2009**, *4* (2), 155−173.
(52) Schindelin, J.; Arganda-Carreras, I.; Frise, E.; Kaynig, V.; Longair, M.; Pietzsch, T.; Preibisch, S.; Rueden, C.; Saalfeld, S.; Schmid, B.; et al. Fiji: an open-source platform for biological-image analysis. *Nat. Methods* **2012**, *9* (7), 676−682.
(53) Brookhouser, N.; Raman, S.; Frisch, C.; Srinivasan, G.; Brafman, D. A. APOE2 mitigates disease-related phenotypes in an isogenic hiPSC-based model of Alzheimer's disease. *Mol. Psychiatry* **2021**, *26* (10), 5715−5732.
(54) Engler, A. J.; Carag-Krieger, C.; Johnson, C. P.; Raab, M.; Tang, H.-Y.; Speicher, D. W.; Sanger, J. W.; Sanger, J. M.; Discher, D. E. Embryonic cardiomyocytes beat best on a matrix with heart-like elasticity: scar-like rigidity inhibits beating. *J. Cell Sci.* **2008**, *121* (22), 3794−3802.
(55) Li, H.; Yu, B.; Yang, P.; Zhan, J.; Fan, X.; Chen, P.; Liao, X.; Ou, C.; Cai, Y.; Chen, M. Injectable AuNP-HA matrix with localized stiffness enhances the formation of gap junction in engrafted human induced pluripotent stem cell-derived cardiomyocytes and promotes cardiac repair. *Biomaterials* **2021**, *279*, 121231.
(56) Wang, Q.; Hou, R.; Cheng, Y.; Fu, J. Super-tough double-network hydrogels reinforced by covalently compositing with silica-nanoparticles. *Soft Matter* **2012**, *8* (22), 6048−6056.
(57) Huang, G.; Wessels, A.; Smith, B.; Linask, K.; Ewart, J.; Lo, C. Alteration in connexin 43 gap junction gene dosage impairs conotruncal heart development. *Dev. Biol.* **1998**, *198* (1), 32−44.
(58) Guan, K.; Fürst, D. O.; Wobus, A. M. Modulation of sarcomere organization during embryonic stem cell-derived cardiomyocyte differentiation. *Eur. J. Cell Biol.* **1999**, *78* (11), 813−823.
(59) You, J.-O.; Rafat, M.; Ye, G. J.; Auguste, D. T. Nanoengineering the heart: conductive scaffolds enhance connexin 43 expression. *Nano Lett.* **2011**, *11* (9), 3643−3648.
(60) Tsui, J. H.; Leonard, A.; Camp, N. D.; Long, J. T.; Nawas, Z. Y.; Chavanachat, R.; Smith, A. S.; Choi, J. S.; Dong, Z.; Ahn, E. H.; et al. Tunable electroconductive decellularized extracellular matrix hydrogels for engineering human cardiac microphysiological systems. *Biomaterials* **2021**, *272*, 120764.
(61) Roshanbinfar, K.; Kolesnik-Gray, M.; Angeloni, M.; Schruefer, S.; Fiedler, M.; Schubert, D. W.; Ferrazzi, F.; Krstic, V.; Engel, F. B. Collagen Hydrogel Containing Polyethylenimine-Gold Nanoparticles for Drug Release and Enhanced Beating Properties of Engineered Cardiac Tissues. *Adv. Healthcare Mater.* **2023**, *12*, 2202408.
(62) Yang, X.; Pabon, L.; Murry, C. E. Engineering adolescence: maturation of human pluripotent stem cell-derived cardiomyocytes. *Circ. Res.* **2014**, *114* (3), 511−523.
(63) Fan, C.; Tang, Y.; Zhao, M.; Lou, X.; Pretorius, D.; Menasche, P.; Zhu, W.; Zhang, J. CHIR99021 and fibroblast growth factor 1 enhance the regenerative potency of human cardiac muscle patch after myocardial infarction in mice. *J. Mol. Cell. Cardiol.* **2020**, *141*, 1−10.
(64) Xu, X. Q.; Soo, S. Y.; Sun, W.; Zweigerdt, R. Global expression profile of highly enriched cardiomyocytes derived from human embryonic stem cells. *Stem Cells* **2009**, *27* (9), 2163−2174.
(65) Johnson, R. D.; Camelliti, P. Role of non-myocyte gap junctions and connexin hemichannels in cardiovascular health and disease: novel therapeutic targets? *Int. J. Mol. Sci.* **2018**, *19* (3), 866.
(66) Churko, J. M.; Garg, P.; Treutlein, B.; Venkatasubramanian, M.; Wu, H.; Lee, J.; Wessells, Q. N.; Chen, S.-Y.; Chen, W.-Y.; Chetal, K.; et al. Defining human cardiac transcription factor hierarchies using integrated single-cell heterogeneity analysis. *Nat. Commun.* **2018**, *9* (1), 4906.
(67) Friedman, C. E.; Nguyen, Q.; Lukowski, S. W.; Helfer, A.; Chiu, H. S.; Miklas, J.; Levy, S.; Suo, S.; Han, J.-D. J.; Osteil, P.; et al. Single-cell transcriptomic analysis of cardiac differentiation from human PSCs reveals HOPX-dependent cardiomyocyte maturation. *Cell Stem Cell* **2018**, *23* (4), 586−598.e8.

https://doi.org/10.1021/acsbiomaterials.3c01256
ACS Biomater. Sci. Eng. 2024, 10, 2351−2366